NASA Technical Memorandum 88969

Experimental Aerodynamic Performance of Advanced 40°-Swept, 10-Blade Propeller Model at Mach 0.6 to 0.85

Glenn A. Mitchell
Lewis Research Center
Cleveland, Ohio

September 1988

NASA

EXPERIMENTAL AERODYNAMIC PERFORMANCE OF ADVANCED 40°-SWEPT, 10-BLADE PROPELLER MODEL AT MACH 0.6 TO 0.85

Glenn A. Mitchell
National Aeronautics and Space Administration
Lewis Research Center
Cleveland, Ohio 44135

SUMMARY

A propeller designated as SR-6 was tested in the NASA Lewis Research Center's 8- by 6-Foot Wind Tunnel. The propeller was one of a series of advanced single-rotation propeller models that were designed and tested as a part of the NASA Advanced Turboprop Project. It was designed with 40° of sweep and 10 blades to cruise at Mach 0.8 at an altitude of 10.7 km (35 000 ft) with a power loading of 241 kW/m^2 (30 hp/ft^2) and a tip speed of 213 m/sec (700 ft/sec). Earlier advanced propellers for this speed and altitude were designed with eight blades for a power loading of 301 kW/m^2 (37.5 hp/ft^2) and a tip speed of 244 m/sec (800 ft/sec).

The propeller model was mounted on the NASA Lewis propeller test rig and tested for aerodynamic performance in the transonic test section of the NASA Lewis 8- by 6-Foot Wind Tunnel at Mach numbers from 0.6 to 0.85 and propeller blade angles from 58.5° to 66.4°.

Basic propeller performance is presented in terms of net efficiency and power coefficient versus advance ratio. Design-point net efficiency was almost constant to Mach 0.75 but fell above this speed more rapidly than that of any previously tested advanced propeller. All portions of the propeller blade appeared to contribute to the compressibility-caused performance loss, including the hub region, where the interblade flow choked. Alternative spinners designed to reduce the near-hub interblade Mach numbers improved propeller performance above Mach 0.75. With the optimum alternative spinner the estimated SR-6 design-point net efficiency was 80.6 percent at Mach 0.75 and 79.2 percent at Mach 0.8, higher than the measured performance of any previously tested advanced single-rotation propeller at these speeds.

INTRODUCTION

Propeller propulsion systems have rather large efficiency advantages over the more highly loaded turbofan propulsion systems. Although these advantages diminish at high subsonic Mach numbers, they are still large. At Mach 0.8, for example, the installed efficiency of an advanced single-rotation turboprop would be about 77 percent, in contrast to about 64 percent for a turbofan system (ref. 1). These installed efficiencies include the installation losses for both systems: namely, nacelle drag for the turboprop systems and cowl drag and fan internal airflow losses for the turbofan systems. Such efficiency comparisons have led to a number of aircraft mission studies by both NASA and industry. These studies indicate that a trip fuel savings of 15 to 30 percent can be achieved for a Mach 0.8 cruise advanced turboprop aircraft over an equivalent-technology turbofan aircraft (refs. 1 and 2).

The NASA Advanced Turboprop (ATP) Project was created to develop and confirm the technologies that will attain these projected fuel savings in complete large-scale engine systems. Supporting technology for this project was supplied in part by the design and testing of advanced propeller models. A series of models of single-rotation propellers designed for cruise operation at Mach 0.8 and 10.7-km (35 000-ft) altitude have been tested by NASA and Hamilton Standard in wind tunnels at the NASA Lewis Research Center and the United Technologies Research Center. Aerodynamic performance test results for the straight-blade SR-2 propeller, the 30°-swept SR-1 propeller, and the 45°-swept SR-3 propeller have been published in references 3 to 7. All of these models were designed by Hamilton Standard under contract to Lewis. The model reported herein (designated SR-6) was aerodynamically designed at Lewis, with Hamilton Standard performing the mechanical design and model fabrication under contract.

An experimental test program to determine the aerodynamic performance of the SR-6 propeller model was conducted in the NASA Lewis 8- by 6-Foot Wind Tunnel at free-stream Mach numbers from 0.6 to 0.85 over a range of propeller blade angles and tip speeds. Basic performance results are presented herein in terms of net efficiency and power coefficient versus advance ratio. Net efficiency rather than installed efficiency is presented since the model tests could not measure real installation losses. These basic data are summarized at each tested free-stream Mach number and analyzed to assess compressibility effects. Limited data are presented for the propeller with alternative spinners designed to relieve hub choking at the higher free-stream Mach numbers. The SR-6 propeller performance is compared with the performances of the earlier propeller models.

APPARATUS AND PROCEDURE

Propeller Design Features

The SR-6 propeller (fig. 1) was designed to cruise at Mach 0.8 at an altitude of 10.7 km (35 000 ft). Its design characteristics (fig. 2) were chosen to obtain high performance and to minimize the propeller source noise. Earlier advanced propellers (SR-1, SR-2, and SR-3) were designed to operate at the same Mach number and altitude. These propellers had eight blades, a design power loading (ratio of shaft horsepower to the square of the reference blade tip diameter SHP/D^2) of 301 kW/m^2 (37.5 hp/ft^2), and a design tip speed of 244 m/sec (800 ft/sec). The design tip speed of the SR-6 was lowered to 213 m/sec (700 ft/sec) to reduce the source noise. The potential performance lost by lowering the tip speed was regained and somewhat improved by increasing the number of blades to 10 and lowering the design power loading to 241 kW/m^2 (30 hp/ft^2). The result of these design changes was a 1 percent increase in ideal induced efficiency.

The aerodynamic blade shape characteristics along the mean flow streamlines are presented for the SR-6 propeller in figure 3. The thickness t/b, twist $\Delta\beta$, design lift coefficient C_{LD}, and chord b/D distributions are shown as functions of blade radius ratio. The blade airfoil types chosen for the SR-6 propeller were the same as those used on the earlier propellers (i.e., NACA series 16 in the outboard sections and NACA series 65 with a circular-arc mean camber line in the inboard sections). Between these was a transition region, as shown in figure 3. The thickness-to-chord ratio t/b distribution

of the SR-6 was the same as that of the earlier propellers except near the hub, as discussed later. The blade chord-to-diameter ratio b/D distribution was similar to that of the earlier propellers SR-1 and SR-2. The design lift coefficient C_{LD} and blade twist $\Delta\beta$ distributions shown in figure 3 were optimized during the design process for maximum efficiency at the design condition: free-stream Mach number, M_0, 0.8; advance ratio, J, 3.5; and power coefficient, C_p, 2.03.

The SR-6 propeller blades were swept to help reduce source noise and lower compressibility losses in order to maintain high efficiency at the high (Mach 0.8) design speed, where local helical Mach numbers on the outer portions of the blade would exceed Mach 1.0. The sweep distribution was determined by keeping the local Mach number normal to the blade midchord line just below the drag divergence Mach number of the airfoil section at each blade radial station. The resulting aerodynamic sweep (fig. 4) has two components. One is the geometric or manufactured sweep shown in the figure. The other is the radial flow angle of the mean-flow streamlines induced by the spinner contour. This component is represented by the difference between the manufactured and aerodynamic sweep. As figure 4 shows, all inboard sweep was due to the radial flow angularity, and most of the outboard sweep was the geometric or manufactured sweep. The geometric sweep is also illustrated by the blade photograph in figure 2. In this definition of sweep the tip sweep is approximately the angle between the blade planform midchord line at the blade tip and a radial line intersecting this line at the tip. The aerodynamic tip sweep of 40° was then obtained by adding on the small flow angle at the tip.

The diameter of a swept propeller varies with blade angle, rotational speed, and blade loading. These changes occur because the blade tip travels out of the axial-radial plane of the blade pitch change axis. Blade angle variations caused small diameter changes for the SR-6 propeller (fig. 5). Changes from rotational speed and loading were not significant. For convenience, all data and plots presented in this report use values derived from a constant (or reference) propeller diameter of 0.696 m (27.4 in.). This is the blade diameter with the blade tip angle at 90° (i.e., with the tip aligned axially).

Since the SR-6 propeller model was designed to be tested on the same propeller test rig as the earlier propellers, the hub diameter remained unchanged. However, the lower power loading of 241 kW/m^2 (30 hp/ft^2), instead of the 301 kW/m^2 (37.5 hp/ft^2) for the earlier propellers, required a larger propeller diameter for a proper geometric scaling. The larger SR-6 propeller blades resulted in a smaller propeller hub-to-tip ratio and a physically smaller hub flow area. These considerations, combined with a closer blade spacing from the 10 blades (instead of the 8 for the earlier propellers), increased the chances of hub flow choking at the higher free-stream Mach numbers.

To help alleviate choking, the propeller blades near the hub were made as thin as possible within structural constraints. At the hub the thickness-to-chord ratio t/b was 0.15 for the SR-6 (fig. 3) in contrast to 0.20 for the SR-1, SR-2, and SR-3. Also a new spinner was designed for the SR-6 propeller model that would reduce the near-hub Mach number in the blade region. The contour and coordinates of this spinner (called the basic spinner) are shown in figure 6. Also shown is the predicted local surface Mach number of the axisymmetric spinner alone without blades. The Mach number near the blade leading edge was reduced from the free-stream value of 0.8 to a local value of 0.6.

Additional information suggesting that hub choking might still be a problem became available after the basic spinner and SR-6 propeller were designed. Therefore two alternative spinners were designed to reduce the near-hub-region Mach number below that provided by the basic spinner. Their contours were constrained to mate to the existing basic contour at the blade pitch change axis (X/R_N = 1.674). Forward of the pitch change axis the lower propeller blade surface was matched to the various spinner contours by using alternative, properly contoured blade insets (fig. 2).

Both alternative spinners significantly reduced the Mach number in the blade region below that of the basic spinner. The alternative spinners achieved a Mach number as low as about 0.57. Alternative spinner 2 was expected to alleviate hub choking best since its minimum Mach number location was further aft of the blade leading edge and closer to the location of maximum blade thickness.

The Mach numbers shown in figure 6 are from an axisymmetric, subsonic potential flow computer code (ref. 8) that was quick running and a good design tool. Comparing these results with a more accurate axisymmetric transonic code containing a boundary layer routine (ref. 9) showed good agreement in locating the minimum Mach number region and just a slight underprediction of the minimum Mach number by the potential flow code. Neither program accounts for the propeller blades.

Test Facilities

The SR-6 propeller model was tested in the Lewis 8- by 6-Foot Wind Tunnel. The transonic test section of this facility is 2.44 m (8 ft) high by 1.83 m (6 ft) wide and about 4.3 m (14 ft) long. Originally constructed as a supersonic tunnel operating from Mach 1.5 to 2.0, the tunnel was subsequently modified for transonic and subsonic operation by perforating the test section walls. The perforations were designed to provide a differential resistance to the crosswall flow. One-inch-diameter holes were drilled in the tunnel wall 60° from the normal to provide greater resistance to inflow than to outflow and thereby minimize the strength of wall-reflected disturbances from the model flow field during transonic operation. The normal operating range of this transonic test section is from Mach 0.36 to 2.0. Additional details of this facility can be found in reference 10.

Propeller testing of the SR-6 was accomplished with the Lewis propeller test rig (PTR) (fig. 7), which was strut mounted from the ceiling of the tunnel test section. Dimensions of the nacelle and forward windscreen are presented in the figure. The model is driven by a three-stage air turbine using high-pressure air at 3.1 MN/m^2 (450 psi) and 366 K (660 °R). The turbine can deliver nearly 746 kW (1000 hp) to the propeller model. The PTR has two separate axial force-measuring systems. The primary system is a rotating balance that measures the thrust and torque of the propeller and spinner. The second system is a thrust-measuring load cell located in the overhead vertical strut. Model parts other than the spinner and blades that are attached to the strut-mounted load cell are shielded from the free-stream tunnel air by the windscreen shown in figure 7. Thrust measurements from both systems are corrected for internal pressure tares.

Extensive static calibrations of the load cell and rotating balance were done, as well as two dynamic calibrations of the rotating balance. The first dynamic calibration, performed with only the spinner installed, measured the effect of rotational speed on the thrust and torque output of the rotating balance under no-load conditions. The second dynamic calibration measured the effect of rotational speed on the thrust output of the rotating balance with the blades and spinner installed. This duplicated the model configuration of the performance test runs. The blade angle was set to produce a near-zero thrust level, and the output of the rotating balance was compared with that of the load cell. Both static and dynamic calibrations were repeated several times before and after the test period, and static calibration checks were performed within the test period.

Internal pressures were measured during the propeller testing at the locations shown in figures 8 and 9. Additional static pressures were measured on the outer surface of the nacelle aft of the model spinner. These nacelle pressure taps were placed in four rows spaced 90° apart around the nacelle circumference. The coordinates of each row are listed in figure 9. Measurements of all these pressures to obtain pressure forces is a necessary step in the process of obtaining net thrust from the balance force readings. The tare test runs are a part of this process. These runs measured forces and pressures on a smooth spinner without propeller blades to obtain spinner and nacelle tare forces. When these forces were properly combined with measured test-point thrust and pressure forces, net thrust and thereby net efficiency were obtained. Details of these procedures can be found in reference 7.

Test Description

The SR-6 propeller model was tested at zero angle of attack at Mach 0.6 to 0.85 and blade angles from 58.5° to 66.4° as shown in table I. The blade angle $\beta_{0.75R}$ was measured as the angle of the airfoil chordline at a propeller radius of 75 percent, where 0° was in the direction of rotation and 90° was aligned directly with the flight direction. At each blade angle/Mach number combination the propeller speed was varied from windmill (no power) to the PTR power limit or the propeller blade shank stress speed limit of 8000 rpm. Each rotational speed setting constituted a test point. Balance thrust and torque and all pressures were measured at each condition. The propeller with the basic spinner was tested at all blade angles and Mach numbers. Testing with the two alternative spinners was limited to a blade angle of 61.5°.

Accuracy problems occurred with both model balance systems. The problem with the rotating balance was its slow thermal drift, which was caused by heat from nearby bearings and precluded a good absolute thrust measurement. The strut load cell was prone to large errors when hot, high-pressure air was brought onboard to power the turbine (fig. 7). Major contributors to this error were a thermal drift from the heated air and the windscreen- and ground-to-load cell interactions. Under unpowered conditions these load cell errors did not occur, and good thrust values were measured.

The balance problems were overcome with a special testing procedure that used measurements from both the rotating balance and the strut load cell. An initial series of test runs were made at each Mach number/blade angle combination in which the load cell thrust was measured at windmill, or unpowered, conditions. These runs established reliable thrust levels at the windmill

conditions. Thrust data were then obtained from the rotating balance in a windmill-power-windmill sequence for each desired test point to obtain a windmill-to-power incremental thrust measurement that minimized any thermal drift between the windmill data points. Properly combining the strut load cell thrust and the rotating balance incremental thrust produced reliable final thrust and ultimately net efficiency values. Further details of this procedure and accompanying equations are given in reference 7.

RESULTS AND DISCUSSION

Basic Propeller Performance

The aerodynamic performance of the SR-6 propeller model with the basic spinner is presented in figures 10 to 14 for free-stream Mach numbers of 0.6, 0.7, 0.75, 0.8, and 0.85, respectively. The data in each figure are plotted against advance ratio J. Each curve shows the performance at a constant blade angle $\beta_{0.75R}$ and was obtained by varying propeller tip speed. Part (a) of each figure presents the power coefficient C_p, part (b) the net efficiency η_{net}, and part (c) the net efficiency fairings without the data points. The power coefficient plots of each figure show lines of constant dimensionless power loading or C_p/J^3 corresponding to 70, 80, 90, and 100 percent of the design power loading. These performance data were faired by adjusting computer-generated curve fits of each test run in conjunction with hand-generated fairings of the summary data in figure 15 to yield smooth consistent trends of efficiency with Mach number, advance ratio, and blade angle.

The net efficiency curves of figures 10 to 14 are typical of propeller data and vary from below the scale near the windmilling advance ratio to a peak and then to lower values with decreasing advance ratio. The curve shape, or performance variation, is directly related to the blade-section angle of attack, which affects the lift-to-drag ratio. It is also related to the blade-section relative Mach number, which varies inversely with advance ratio. At the peak efficiencies the blade is generally operating near the maximum lift-to-drag ratio.

Peak efficiency generally occurred at an advance ratio of 3.5 (design) to 3.6. The peak efficiency trend with free-stream Mach number clearly shows the deleterious effect of increasing high-speed compressibility drag. The peak net efficiency fell slowly from 82.2 percent at Mach 0.6 (fig. 10(c)) to 81.2 percent at Mach 0.75 (fig. 12(c)) and then fell rapidly to 78.5 percent at Mach 0.8 (fig. 13(c)) and on to 74.7 percent at Mach 0.85 (fig. 14(c)).

In general, the power coefficient curves for a given blade angle are displaced to the left as the Mach number increases. This reflects the fact that the propeller absorbed less power with increasing Mach number at a fixed blade angle and advance ratio. At the lower tested Mach numbers the curves show moderate reductions in power at a fixed blade angle and advance ratio. These reductions got larger at the higher Mach numbers because of increasing compressibility effects. For example, at a blade angle of 61.5° and an advance ratio of 3.5 the power coefficient dropped from 1.69 to 1.63 as the Mach number increased from 0.6 to 0.75, to 1.49 at Mach 0.8, and then to 1.07 at Mach 0.85. Similar trends are observed in reference 6 and primarily indicate a loss of blade lift due to high transonic speed effects at the higher Mach numbers.

At the same fixed blade angle and advance ratio the SR-6 propeller operated farther from the peak efficiency and lower on the efficiency curve as the Mach number increased from 0.75 to 0.85 (figs. 12(c) and 14(c)). Operating away from the peak in this manner also indicates a loss of lift. Regaining the lost power and raising the efficiency back toward peak would require an increase in blade angle or tip speed. This off-peak efficiency loss is in addition to the compressibility drag losses that were earlier shown to reduce peak efficiency at the higher Mach numbers.

Summary of Basic Performance

The basic propeller data of figures 10 to 14 are summarized in figure 15. For each free-stream Mach number net efficiency is plotted against advance ratio at constant dimensionless power loadings representing 70, 80, 90, and 100 percent of the design power loading. The dimensionless power loading is based on the approximation that the power required for an airplane in level flight is proportional to the cube of the free-stream velocity (i.e., $P/\rho_0 V_0^3 = \text{Constant}$). For a propeller the dimensionless power loading

$$\frac{C_p}{J^3} = \frac{\dfrac{P}{\rho_0 n^3 D^5}}{\dfrac{V_0^3}{n^3 D^3}} = \frac{\dfrac{P}{D^2}}{\rho_0 V_0^3} = \text{Constant}$$

is the ordinary power loading (normally defined in terms of SHP/D^2 rather than P/D^2) nondimensionalized to account for density and velocity changes.

The symbols in figure 15 identify the blade angles and the net efficiency values that were obtained from the computer curve fits of the individual basic data runs prior to the previously discussed fairing adjustments. Thus the discrepancies between the symbols and curves in this figure illustrate the run-to-run variations in the efficiency measurements. The aim of the fairing technique was to eliminate these variations, which appear to be on the order of 1 percent for some of the test runs. Generally the net efficiency trends with Mach number within a single run were quite consistent, and the variations were much smaller than those observed from run to run.

The typical variation of efficiency with advance ratio at a constant power loading is a peaked curve. Generally, the curves of figure 15 peak near the design advance ratio of 3.5, where the lift-to-drag ratio is maximized at the cruise design point. Contributing to the peaked curve shape is the lower lift-to-drag ratio on either side of this optimum. However, the primary cause of the reduction from peak with increasing advance ratio is the falling tip (or rotational) speed, which increases the blade swirl and tip induced losses and lowers the ideal induced efficiency. The falloff with decreasing advance ratio is primarily due to the greater compressibility losses associated with the higher blade-section Mach numbers. At the higher free-stream Mach numbers, an added cause may be hub choking due to the smaller hub flow area (smaller gap-to-chord ratio) from the smaller blade angles at lower advance ratios. In more succinct terms, reductions to the right of peak are mostly from induced losses and reductions to the left are from higher drag or compressibility losses.

The performance trends of the SR-6 propeller shown in figure 15 indicate that at the lower tested Mach numbers and higher advance ratios, a reduction in power loading increased efficiency. The operating point on the basic efficiency curves (fig. 10(c), e.g.) was shifted from left to right toward the peak of the curve. This trend reversed at higher Mach numbers and lower advance ratios, where operation at lower power loadings reduced efficiency. The operating point on the basic efficiency curves (fig. 14(c)) was shifted from left to right but away from the peak.

On the basis of previous high-speed propeller tests, increases in efficiency were expected to be available by operating the propeller away from the design condition of 100-percent power loading and 3.5 advance ratio at a lower power loading. With the SR-6 propeller the efficiency increases obtained by operating in this manner were small to nonexistent and depended on the free-stream Mach number. For example, operating the propeller at 80-percent dimensionless power loading could increase efficiency by 1.2 percent at Mach 0.6 (fig. 15(a)). But increases were more limited at higher Mach numbers: at Mach 0.85 operating at 80-percent dimensionless power loading could increase efficiency only about 0.2 percent, and a lower power loading operation at Mach 0.85 would lose efficiency (fig. 15(e)).

The 100-percent dimensionless power loading curves of figure 15 were replotted in figure 16 to compare the propeller performance at different free-stream Mach numbers. These curves show that propeller efficiency was practically identical at Mach 0.6 and 0.7. Compressibility effects did not increase drag at these Mach numbers. At Mach 0.75 the efficiency was still about the same as at the lower Mach numbers -- but only above an advance ratio of 3.5. Below this advance ratio the efficiency fell below that obtained at the lower Mach numbers. At the higher speed of Mach 0.8 the efficiency was close to that at lower speeds only above an advance ratio of 3.7. Below this advance ratio the efficiency was considerably lower than the efficiencies obtained at the lower Mach numbers. At Mach 0.85 the efficiency was well below that obtained at lower speeds regardless of advance ratio.

These results show that the propeller compressibility losses began at lower advance ratios at about Mach 0.75 and that the losses encompassed higher advance ratios as the free-stream Mach number increased. This trend would be expected since the blade-section Mach numbers are higher at lower advance ratios and higher free-stream Mach numbers. Also, at the lower advance ratios smaller hub gap-to-chord ratios (from smaller blade angles) contribute to the chances of hub choking.

Compressibility Loss Correlations

The compressibility losses incurred by the SR-6 propeller at the higher Mach numbers were not unexpected, but they were larger than anticipated. Was any specific region of the propeller blade primarily responsible for these losses? The performance data of figure 16 were used in an attempt to answer this question. Figure 17 is a replot of the figure 16 data and presents net efficiency against free-stream Mach number for various values of advance ratio. This figure shows explicitly the sudden efficiency decline as the Mach number increased into the higher speed regimes. Plots similar to figure 17 were also made to show net efficiency trends for the helical Mach numbers at various blade radial locations. Net efficiency is presented against helical

tip Mach number, helical Mach number at 75-percent blade radius, and helical hub Mach number (figs. 18 to 20).

The definitions of these helical Mach numbers are given in the appendix and are valid in the outer portions of the propeller blade. However, in the hub region, where the flow is highly three dimensional from hub surface curvature and strongly influenced by cascade effects from the closely spaced blades, the definitions are an oversimplification of the complex near-hub airflow. Despite this, the defined hub helical Mach number appears to be a good representation of the complex hub flow since the data of figure 20 exhibit meaningful and reasonable trends as later discussion shows.

In figures 17 to 20 the Mach number at which the efficiency began to decline is defined for each advance ratio curve as the point where the efficiency level dropped by 0.2 percent. These Mach number points are indicated by the arrows on each figure. The Mach number trend of the efficiency decline with advance ratio can be determined by examining the shift and spacing of the arrows.

Figure 17 shows that the free-stream Mach number at which the efficiency declined increased with increasing advance ratio. This is of course the same trend that was shown by figure 16 and, as explained earlier, occurred because the higher blade-section Mach numbers and smaller hub gap-to-chord ratios that could cause higher compressibility losses occurred at the lower advance ratios.

Figure 18 shows that the helical tip Mach number at which the efficiency declined decreased with increasing advance ratio. If the efficiency had declined at the same tip Mach number regardless of the advance ratio, tip effects would be solely responsible for the efficiency decline. Since there is a trend, more inboard portions of the blade were contributing to the performance decline.

Figure 19 shows that for the helical Mach number at 75-percent blade radius the efficiency declined at nearly the same Mach number regardless of the advance ratio. One interpretation of these data is that the drag rise, or drag divergence, of the specific portions of the blade near the 75-percent blade radius controlled the point of efficiency decline. More probably, all portions of the blade contributed to the decline. This view agrees with common practice wherein conditions at the 75-percent radius generally represent the blade performance as a whole. Thus all parts of the blade (hub as well as tip) contributed to the compressibility drag losses that caused the performance decline. This view is strengthened by the fact that data presented later show that hub choking did in fact occur and that hub region changes from using alternative spinners affected performance.

Figure 20 shows that the helical hub Mach number at which the efficiency declined increased with increasing advance ratio. This trend can be interpreted as showing that the more outer portions of the blade contributed to the efficiency decline. On the other hand, lower advance ratios mean smaller blade angles and smaller hub flow areas from reduced hub gap-to-chord ratios. These could precipitate possible hub choking at a lower helical hub Mach number. Both explanations probably contribute to the observed trend.

Evidence for hub choking with this propeller is reported in reference 11, and a figure from that report is reproduced herein as figure 21. Flow visualization via a paint flow technique was used to display the extent of choking in the interblade region near the hub. The photographs show the SR-6 propeller operating near its design point. A rather extensive shock structure can be seen on both the pressure and suction sides of the propeller blade, indicating that hub choking was quite severe for the condition shown and propagated outward over a considerable portion of the blade span.

From these data it appears that no particular portion of the propeller blade was primarily responsible for the performance decline at the higher free-stream Mach numbers. Certainly hub choking was a substantial contributor. Also, midblade regions may not have performed at optimum in that they may have been into drag rise because of imperfect design and prediction computer codes. In addition, sweep may not have been as effective as predicted. Recall that the power coefficient curves shifted with free-stream Mach number, indicating a loss of lift at the higher free-stream Mach numbers. It appears that the outer, swept portions of the blade as well as the midsections did not operate subcritically as designed.

Performance With Alternative Spinners

The SR-6 propeller performance obtained with the two alternative spinners was compared with the performance obtained with the basic spinner (fig. 22). These data show net efficiency versus free-stream Mach number at a dimensionless power loading of 100 percent with the propeller operating at a blade angle of 61.5°. The comparison is made at this specific blade angle rather than at a specific advance ratio because alternative spinner data were obtained only at this blade angle. Caution must therefore be used in interpreting the net efficiency levels of the alternative spinner data. Since only a single data run at the blade angle of 61.5° was made for each alternative spinner, run-to-run data level variations such as those shown in figure 15 for the basic spinner configuration may be present. Moreover, only a single windmill drag run (explained earlier under the section "Test Description") was available for data reduction of alternative spinner 1, adding to the data uncertainty since an average of four windmill drag runs was normally used.

In spite of these shortcomings the trends with free-stream Mach number shown in figure 22 are without scatter and seem quite consistent, as they were for the basic spinner data presented earlier. These trends contain the important information on performance, which was extracted as follows: For each spinner design there was no change in propeller efficiency between Mach 0.6 and 0.7. At these lower speeds, where compressibility effects were not present, the spinner configuration would not be expected to alter performance. Therefore all the efficiency levels at Mach 0.6 and 0.7 in figure 22 were assumed to be identical, and the data were so normalized and presented in figure 23 as an efficiency change with free-stream Mach number. Thus the trends of figure 22 are preserved, and figure 23 more closely represents the true comparative performance of the propeller with various spinners.

Figure 23 shows that the alternative spinners improved the propeller performance over that achieved with the basic spinner at the higher free-stream Mach numbers, where compressibility effects were causing a decrease in net efficiency. Since the alternative spinners reduced the near-hub Mach number

in the blade region (fig. 6), their effect on performance was due to some relief of the interblade hub choking phenomenon illustrated by the shock structure of figure 21. As expected, alternative spinner 2 was best at improving the net efficiency at Mach 0.8 and 0.85, just about doubling the improvement obtained by alternative spinner 1. As explained earlier with figure 6, alternative spinner 2 would best alleviate choking since its minimum Mach number region was at a more optimum location.

Performance Comparison

Figure 24 compares the performance of the 10-blade SR-6 propeller with that of the previously tested 8-blade SR-1M, SR-2, and SR-3 propellers. The SR-1M was a retwisted version of the SR-1, as explained in reference 4. Net efficiency is plotted in the figure versus free-stream Mach number for each propeller operating at its design power coefficient C_p and advance ratio J (i.e., at 100 percent of its dimensionless power loading at design conditions). Since power coefficient and advance ratio were constant for each propeller across the Mach number range, the ideal induced efficiency (ref. 12) was also constant for each propeller. Figure 24 shows that the ideal induced efficiency of the SR-6 propeller was about 1 percent higher than that of the other propellers. The ideal induced efficiency represents the performance of an optimally loaded propeller with no blade drag. Because figure 24 presents the performance of each propeller at its design conditions, the difference between the ideal induced efficiency and the experimental net efficiency of each propeller represents the drag and compressibility losses. These are shown in the figure to increase with increasing free-stream Mach number.

The estimated performance presented in figure 24 for the SR-6 propeller with alternative spinner 2 was obtained by adding the efficiency increments from figure 23 to the SR-6 basic spinner performance curve of figure 24. This approximation seems valid since propeller operation at the 61.5° blade angle at 100-percent dimensionless power loading for the different spinner shapes occurred at an advance ratio relatively close to the design value of 3.5. Note that the basic SR-6 performance curve shown in figure 24 is a replot of the net efficiency curve at an advance ratio of 3.5 from figure 17.

The SR-1M, SR-2, and SR-3 propellers were previously compared in references 1 and 4. The straight-blade SR-2 propeller had the lowest performance and the 45°-swept SR-3 propeller had the best performance among the 8-blade propellers at the higher free-stream Mach numbers of 0.8 and 0.85. These propellers were designed for the same power loading and tip speed. The results show that sweep is effective in reducing compressibility losses in the outer portions of the propeller blade, thereby increasing efficiency at the higher free-stream Mach numbers.

A comparison of the SR-6 propeller performance with the performance of the 8-blade propellers must account for the 1-percent induced efficiency advantage of the SR-6. The SR-6 propeller did not realize this potential efficiency advantage over the other propellers at the lower free-stream Mach numbers of 0.6 and 0.7 (fig. 24). The SR-6 net efficiency of 80.7 percent was about 0.4 percent above that of the SR-3 propeller but about 0.5 to 0.6 percent below that of the SR-1M propeller. However, the performances of the other propellers began to fall off above Mach 0.7 whereas the performance of the SR-6 was relatively constant to beyond Mach 0.75. Because of this, the performance of

the SR-6 at Mach 0.75 was better than that of the other propellers. Its net efficiency of 80.5 percent was 0.5 to 0.7 percent above the performance levels of the two 8-blade swept propellers. Here the SR-6 successfully delayed compressibility losses and recorded the highest design-point net efficiency yet obtained at Mach 0.75. At the higher free-stream Mach numbers of 0.8 and 0.85, hub choking sharply decreased the SR-6 performance. Also, as mentioned earlier, sweep may not be as effective at the higher Mach numbers as predicted, and the swept portions of the blade may not be operating subcritically as designed. The net efficiency fell more rapidly with Mach number than that for the other propellers, reaching 78 percent at Mach 0.8 and falling to 74.3 percent at Mach 0.85. These efficiencies were below those of the other propellers except the straight-blade SR-2.

With alternative spinner 2 installed to help alleviate hub choking, the performance estimated for the SR-6 propeller showed a significant improvement over the performance of the basic SR-6 configuration at the higher free-stream Mach numbers. Net efficiency was increased by 1.2 percent at Mach 0.8 and by 2.0 percent at Mach 0.85. Although still below the net efficiency of the SR-3 propeller at Mach 0.85, the estimated design point net efficiencies of the SR-6 propeller with alternative spinner 2 were higher than any efficiency yet obtained for any single-rotation propeller model at Mach 0.75 and 0.8. These net efficiencies were 80.2 percent at Mach 0.75 and 79.2 percent at Mach 0.8 and represent estimated efficiency improvements over previous propeller performance of 0.6 and 0.5 percent, respectively.

SUMMARY OF RESULTS

A 10-blade, 40°-swept, advanced Mach 0.8 propeller model, designated SR-6, was designed and wind tunnel tested to determine its aerodynamic performance. This effort continues a series of single-rotation propeller model tests providing supporting technology to the Advanced Turboprop Project. The SR-6 design tip speed of 213 m/sec (700 ft/sec) was reduced from the 244-m/sec (800-ft/sec) tip speed of the previously designed advanced propellers to reduce source noise. Also the SR-6 had 10 blades rather than 8 and a lower power loading than the previous designs: 241 kW/m^2 (30 hp/ft^2) versus 301 kW/m^2 (37.5 hp/ft^2) at the cruise altitude of 10.7 km (35 000 ft). With these changes the SR-6 had a 1 percent advantage in ideal induced efficiency. In addition to a basic spinner design, two alternative spinners were designed to further reduce the interblade Mach number near the hub and to help alleviate any hub choking that might occur at the higher test Mach numbers.

The propeller model was mounted on the Lewis propeller test rig and tested for aerodynamic performance in the transonic test section of the Lewis 8- by 6-Foot Wind Tunnel. Propeller testing using the basic spinner was conducted at zero angle of attack over a range of free-stream Mach numbers from 0.6 to 0.85 at propeller blade angles from 58.5° to 66.4°. Testing with the alternative spinners was limited to a blade angle of 61.5°. The following results were obtained:

1. With the basic spinner the propeller design-point net efficiency was 80.7 percent at Mach 0.6 and 0.7 and was almost constant up to a free-stream Mach number of 0.75, where a net efficiency of 80.5 percent was obtained. At the higher Mach numbers of 0.8 and 0.85 the performance fell rapidly (more rapidly than for any previously tested advanced propeller) to net efficiencies

of 78 percent and 74.3 percent, respectively. When compared with the design-point net efficiencies of the previously tested advanced propellers, the net efficiency of the SR-6 was higher only at Mach 0.75.

2. The observed rapid decline in net efficiency that occurred as a result of compressibility effects at the higher free-stream Mach numbers was evaluated against the local blade Mach number at various radial stations for evidence of correlation. Results of these comparisons indicate that no particular portion of the blade was primarily responsible for the compressibility-caused performance decline.

3. Choking of the interblade flow near the hub was a contributor to the rapid SR-6 performance decline as evidenced by flow visualization of an extensive interblade near-hub shock structure. Also, improved propeller performance above Mach 0.75 was indicated by limited propeller data obtained using alternative spinners with contours that reduced the near-hub interblade Mach numbers and relieved the choking.

4. Performance data obtained with a more optimum alternative spinner indicated that the basic SR-6 net efficiency was increased 1.2 percent at Mach 0.8 and 2.0 percent at Mach 0.85. With this spinner the estimated SR-6 design-point net efficiency was 80.6 percent at Mach 0.75 and 79.2 percent at Mach 0.8, higher than the measured performance of any previously tested advanced single-rotation propeller at these speeds.

REFERENCES

1. Mikkelson, D.C.; Mitchell, G.A.; and Bober, L.J.: Summary of Recent NASA Propeller Research. NASA TM-83733, 1984.

2. Whitlow, J.B., Jr.; and Sievers, G.K.: Fuel Savings Potential of the NASA Advanced Turboprop Program. NASA TM-83736, 1984.

3. Mikkelson, D.C.; et al.: Design and Performance of Energy Efficient Propellers for Mach 0.8 Cruise. SAE Paper 770458, Mar. 1977. (NASA TM X-73612.)

4. Jeracki, R.J.; Mikkelson, D.C.; and Blaha, B.J.: Wind Tunnel Performance of Four Energy Efficient Propellers Designed for Mach 0.8 Cruise. SAE Paper 790573, Apr. 1979. (NASA TM-79124.)

5. Black, D.M; Menthe, R.W.; and Wainauski, H.S.: Design and Performance Testing of an Advanced 30° Swept, Eight Bladed Propeller at Mach Numbers from 0.2 to 0.85. NASA CR-3047, 1978.

6. Rohrbach, C.; et al.: Evaluation of Wind Tunnel Performance Testings of an Advanced 45° Swept Eight-Bladed Propeller at Mach Numbers from 0.45 to 0.85. NASA CR-3505, 1982.

7. Stefko, G.L.; and Jeracki, R.J.: Wind Tunnel Performance of Two Advanced High Speed Propellers at Takeoff, Climb, and Landing Mach Numbers. NASA TM-87030, 1985.

8. Hess, J.L.; and Smith, A.M.O.: Calculation of Potential Flow About Arbitrary Bodies. Progress in Aeronautical Sciences, Vol. 8, D. Kuchemann, ed., Pergamon Press, 1967, pp. 1-138.

9. Chow, W.L.; Bober, L.J.; and Anderson, B.H.: Numerical Calculation of Transonic Boattail Flow. NASA TN D-7984, 1975.

10. Swallow, R.J.; and Aiello, R.A.: NASA Lewis 8- by 6-Foot Supersonic Wind Tunnel. NASA TM X-71542, 1974.

11. Stefko, G.L.; Bober, L.J.; and Neumann, H.E.: New Test Techniques and Analytical Procedures for Understanding the Behavior of Advanced Propellers. NASA TM-83360, 1983.

12. Standard Method of Propeller Performance Estimation, Society of British Aircraft Constructors, London, 1939.

APPENDIX - SYMBOLS

AF blade activity factor, $6250 \int_{hub}^{x=1.0} (b/D)x^3 \, dx$

b elemental blade chord, cm (in.)

C_{LD} elemental blade design lift coefficient

C_{Li} integrated design lift coefficient, $\int_{hub}^{x=1.0} C_{LD}x^3 \, dx$

C_p power coefficient, $P/\rho_0 n^3 D^5$

D reference blade tip diameter, 0.696 m (27.4 in., or 2.283 ft for J and C_p)

J advance ratio, V_0/nD

M_{hh} helical hub Mach number, $M_0\sqrt{\left(\frac{V}{V_0}\right)^2_{hub} + \left[\left(\frac{r}{R}\right)_{hub}\left(\frac{\pi}{J}\right)\right]^2}$

M_{ht} helical tip Mach number, $M_0\sqrt{1 + \left(\frac{\pi}{J}\right)^2}$

M_ℓ local Mach number

M_0 free-stream Mach number

$M_{0.75R}$ helical Mach number at 75-percent blade radius,

$$M_0\sqrt{\left(\frac{V}{V_0}\right)^2_{0.75R} + \left[\left(\frac{r}{R}\right)_{0.75R}\left(\frac{\pi}{J}\right)\right]^2}$$

n	rotational speed, rps
P	power, W (ft-lb/sec)
R	reference blade tip radius, cm (in.)
R_N	nacelle maximum radius, 11.05 cm (4.35 in.)
r	radius, cm (in.)
SHP	shaft power, kW (hp)
T	thrust, N (lbf)
t	elemental blade maximum thickness, cm (in.)
V	velocity, m/sec (ft/sec)
V_0	free-stream velocity, m/sec (ft/sec)
X	axial length, cm (in.)
x	radius ratio, r/R
$\beta_{0.75R}$	propeller blade angle at 75-percent radius, deg
$\Delta\beta$	blade twist
η_{net}	net efficiency, $T_{net}V_0/P$
θ	circumferential position, deg
ρ_0	free-stream density, kg/m^3 ($slugs/ft^3$)

TABLE I. - TEST MATRIX

[Each symbol denotes a separate test run. These symbols identify blade angles in data figures.]

Blade angle, $\beta_{0.75R}$	Free-stream Mach number				
	0.6	0.7	0.75	0.8	0.85
58.5	∩	∩	∩	∩	∩
59.5	◿	◿	◿	◿	◿
60.8	◢	◢	◢	◢	◢
61.5	△ ▷ ▽	△ ▽	△ ▽	△ ▷ ▽	△
63.0	◇	◇	◇	◇	◇
64.6	□	□	□	□	□
66.4	○	○	○	○	○

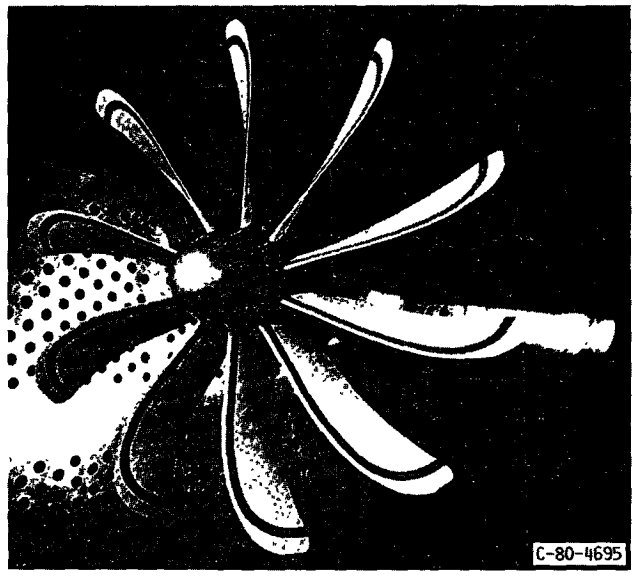

FIGURE 1. - SR-6 10-BLADE PROPELLER MODEL INSTALLED IN LEWIS 8-BY 6-FOOT WIND TUNNEL.

NUMBER OF BLADES	10
TIP SWEEP ANGLE, DEG	40
MODEL DIAMETER, D, CM (IN.)	69.6 (27.4)
ACTIVITY FACTOR, AF	204
INTEGRATED DESIGN LIFT COEFFICIENT, C_{Li}	0.192
AIRFOILS	NACA 16 SERIES, AND 65 SERIES WITH CIRCULAR ARC (CA) CAMBER
RATIO OF NACELLE MAXIMUM DIAMETER TO PROPELLER DIAMETER	0.318
PROPELLER HUB-TO-TIP RATIO	0.214
CRUISE DESIGN MACH NUMBER	0.8
CRUISE DESIGN ALTITUDE, KM (FT)	10.7 (35 000)
CRUISE DESIGN TIP SPEED, M/SEC (FT/SEC)	213 (700)
CRUISE DESIGN POWER LOADING, SHP/D^2, kW/M^2 (HP/FT^2)	241 (30)
CRUISE DESIGN ADVANCE RATIO, J	3.5
CRUISE DESIGN POWER COEFFICIENT, C_p	2.03

PROPELLER
BLADE PLANFORM

FIGURE 2. - SR-6 PROPELLER DESIGN CHARACTERISTICS AND BLADE PLANFORM.

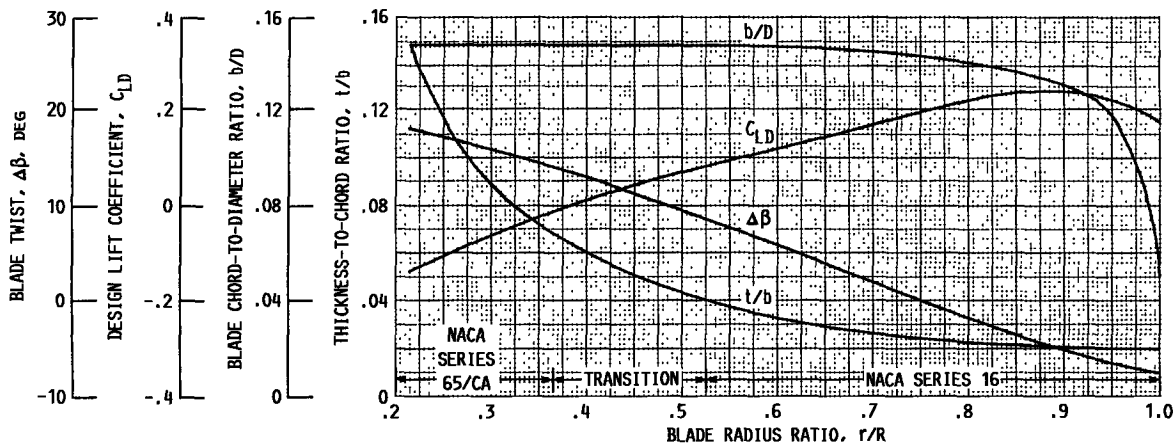

FIGURE 3. - BLADE CHARACTERISTICS.

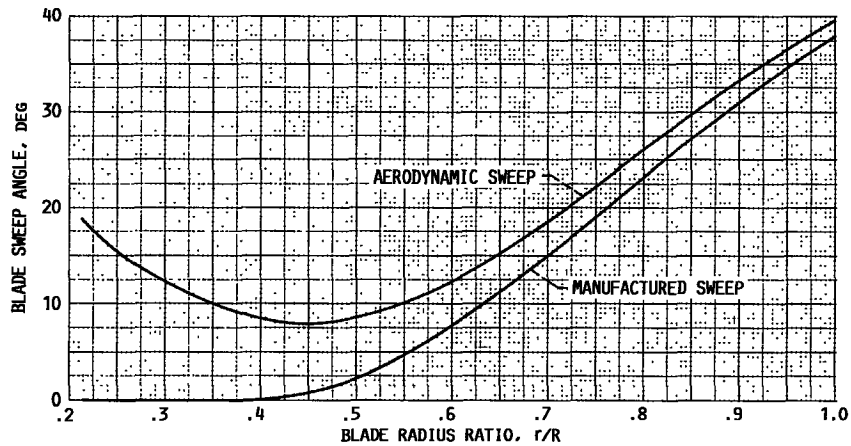

FIGURE 4. - BLADE SWEEP DISTRIBUTION.

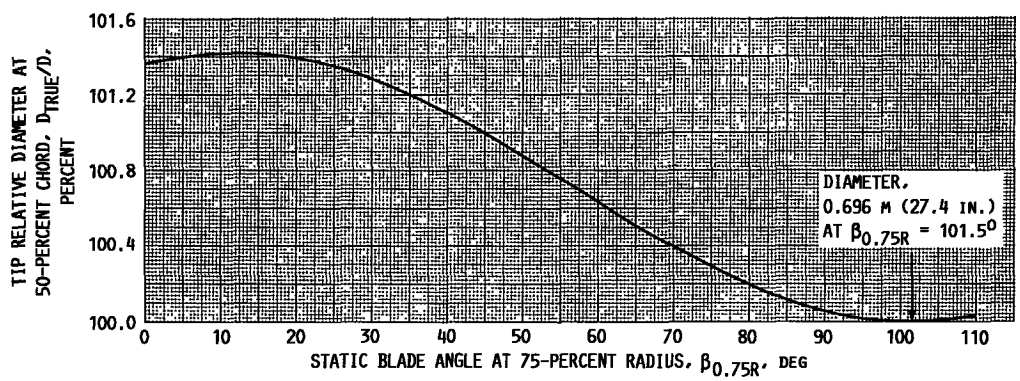

FIGURE 5. - EFFECT OF BLADE ANGLE ON TIP DIAMETER.

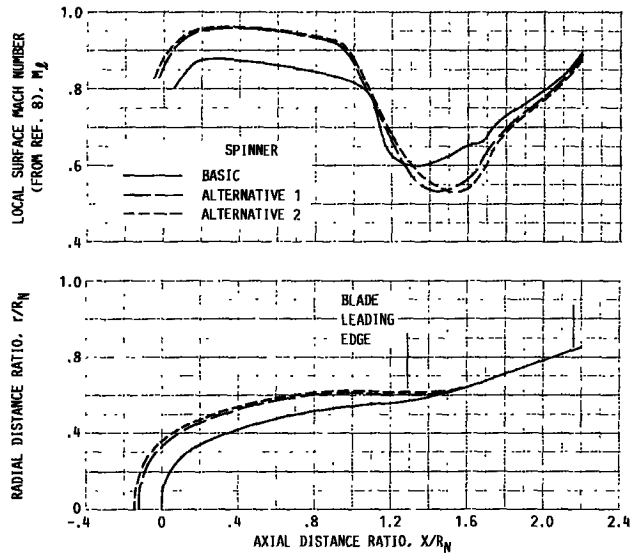

BASIC SPINNER		ALTERNATIVE SPINNER 1		ALTERNATIVE SPINNER 2	
X/R_N	r/R_N	X/R_N	r/R_N	X/R_N	r/R_N
0	0	-0.120	0	-0.143	0
.001	.057	-.119	.053	-.142	.054
.008	.115	-.116	.099	-.139	.100
.025	.171	-.108	.145	-.131	.147
.055	.222	-.097	.186	-.120	.188
.092	.262	-.085	.214	-.097	.240
.138	.300	-.062	.256	-.074	.276
.184	.329	-.039	.288	-.039	.318
.230	.354	-.005	.326	-.005	.351
.287	.380	.030	.357	.030	.379
.345	.402	.064	.383	.064	.403
.402	.422	.099	.405	.099	.423
.460	.440	.133	.425	.133	.442
.517	.456	.179	.448	.179	.464
.575	.470	.225	.469	.225	.484
.632	.483	.271	.487	.271	.501
.690	.495	.317	.503	.317	.517
.747	.506	.363	.518	.363	.531
.805	.517	.409	.531	.409	.544
.862	.526	.455	.543	.455	.556
.920	.534	.501	.554	.501	.566
.982	.542	.547	.564	.547	.576
1.044	.549	.593	.572	.593	.585
1.106	.553	.639	.580	.639	.592
1.149	.554	.685	.587	.685	.599
1.207	.558	.731	.593	.731	.605
1.264	.565	.777	.598	.777	.610
1.322	.574	.823	.603	.823	.614
1.379	.585	.869	.606	.869	.617
1.437	.599	.915	.608	.915	.620
1.494	.614	.961	.609	.961	.621
1.552	.631	1.007	.609	1.007	.620
1.609	.648	1.053	.607	1.053	.618
1.663	.666	1.099	.605	1.099	.616
1.674	.669	1.145	.602	1.145	614
1.685	.673	1.191	.600	1.191	.611
1.743	.694	1.237	.598	1.237	.610
1.857	.735	1.283	.598	1.283	.609
1.972	.776	1.329	.599	1.329	.610
2.087	.817	1.375	.602	1.375	.612
2.202	.857	1.421	.607	1.421	.616
		1.467	.614	1.467	.621
		1.513	.623	1.513	.628
		1.522	.625	1.559	.637
		(a)		1.568	.639
				(a)	

[a]REMAINING COORDINATES ARE THE SAME AS THOSE OF THE BASIC SPINNER.

FIGURE 6. - SPINNER CONTOURS AND SURFACE MACH NUMBER DISTRIBUTIONS AT FREE-STREAM MACH NUMBER M_0 OF 0.8.

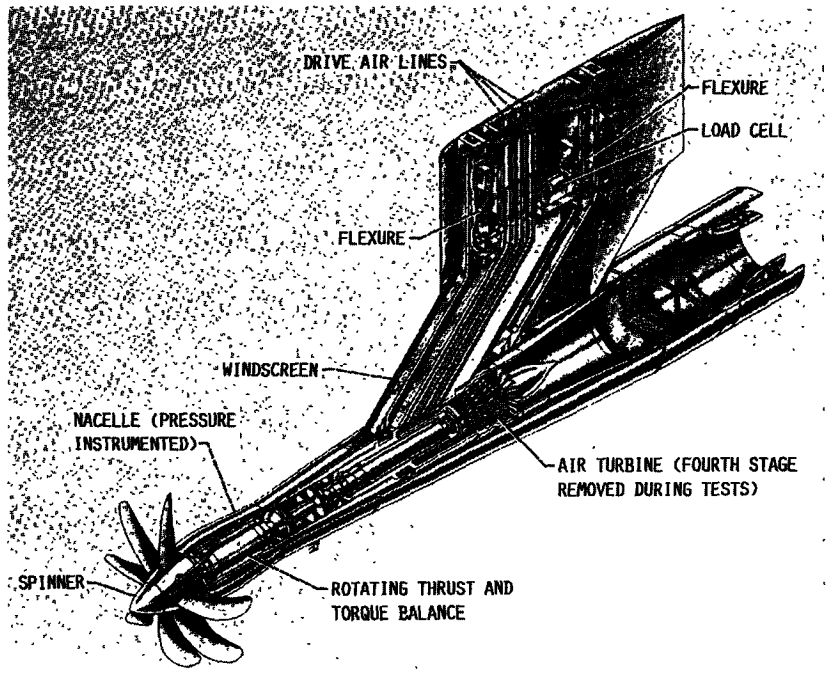

NACELLE DIMENSIONS

X/R_N	r/R_N	X/R_N	r/R_N
2.208	0.860	2.915	0.990
2.225	.866	3.145	.999
2.248	.873	3.223	1.000
2.271	.881	3.375	.999
2.294	.888	3.605	.990
2.317	.895	3.834	.975
2.340	.902	4.064	.956
2.363	.908	4.294	.933
2.386	.915	4.524	.911
2.409	.920	4.754	.894
2.432	.926	4.984	.883
2.455	.931	5.214	.874
2.570	.953	5.260	.873
2.685	.970	5.306	.872
2.800	.982	5.409	.871

WINDSCREEN DIMENSIONS

X/R_N	r/R_N
5.426	0.865
8.668	[a]1.046

[a]STRAIGHT LINE.

FIGURE 7. - CUTAWAY VIEW OF LEWIS 1000-HP (746-KW) PROPELLER TEST RIG.

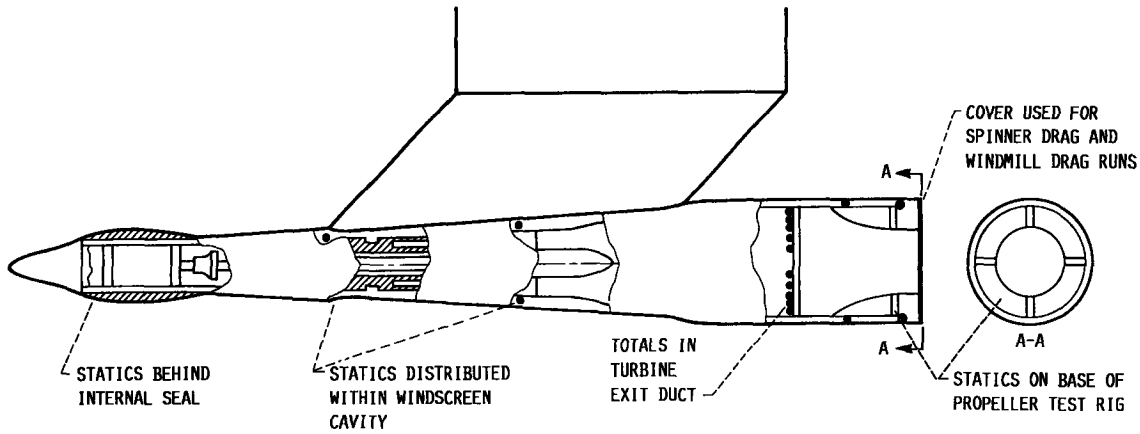

FIGURE 8. - LOCATIONS OF INTERNAL STATIC PRESSURE TAPS.

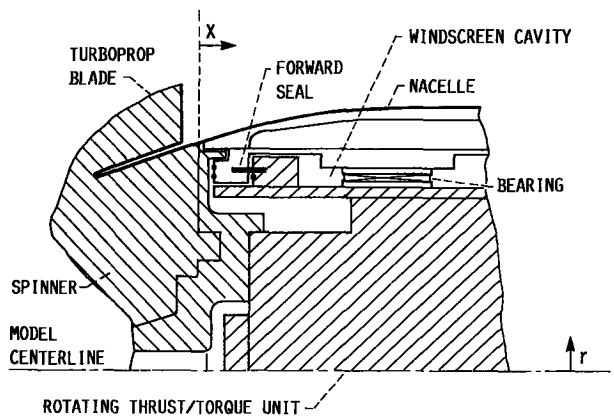

SPINNER STATICS

[R_N = 11.05 cm (4.35 in.).]

r/R_N	θ, DEG
0.6835	0, 180
[a].7353	↓
.7381	
.7861	
.8673	0, 90, 180, 270

[a]BELOW FORWARD SEAL.

NACELLE STATICS

[R_N = 11.05 cm (4.35 in.).]

X/R_N	r/R_N
0.0241	0.8684
.0749	.8848
.1299	.9010
.1880	.9170
.2547	.9326
.3345	.9480
.4276	.9361
.5520	.9780
.7598	.9927
1.0149	1.0000
1.2876	.9949
1.4793	.9848
1.6299	.9745
1.7644	.9642
1.8823	.9537
1.9924	.9431
2.0954	.9323
2.2057	.9215
2.3264	.9105
2.4667	.8994
2.6586	.8882
2.9184	.8768

FIGURE 9. - LOCATIONS OF STATIC PRESSURE TAPS ON NACELLE AND SPINNER FACE.

(a) POWER COEFFICIENT; M_0 = 0.6.

FIGURE 10. - MEASURED PROPELLER PERFORMANCE AT FREE-STREAM MACH NUMBER M_0 OF 0.6.

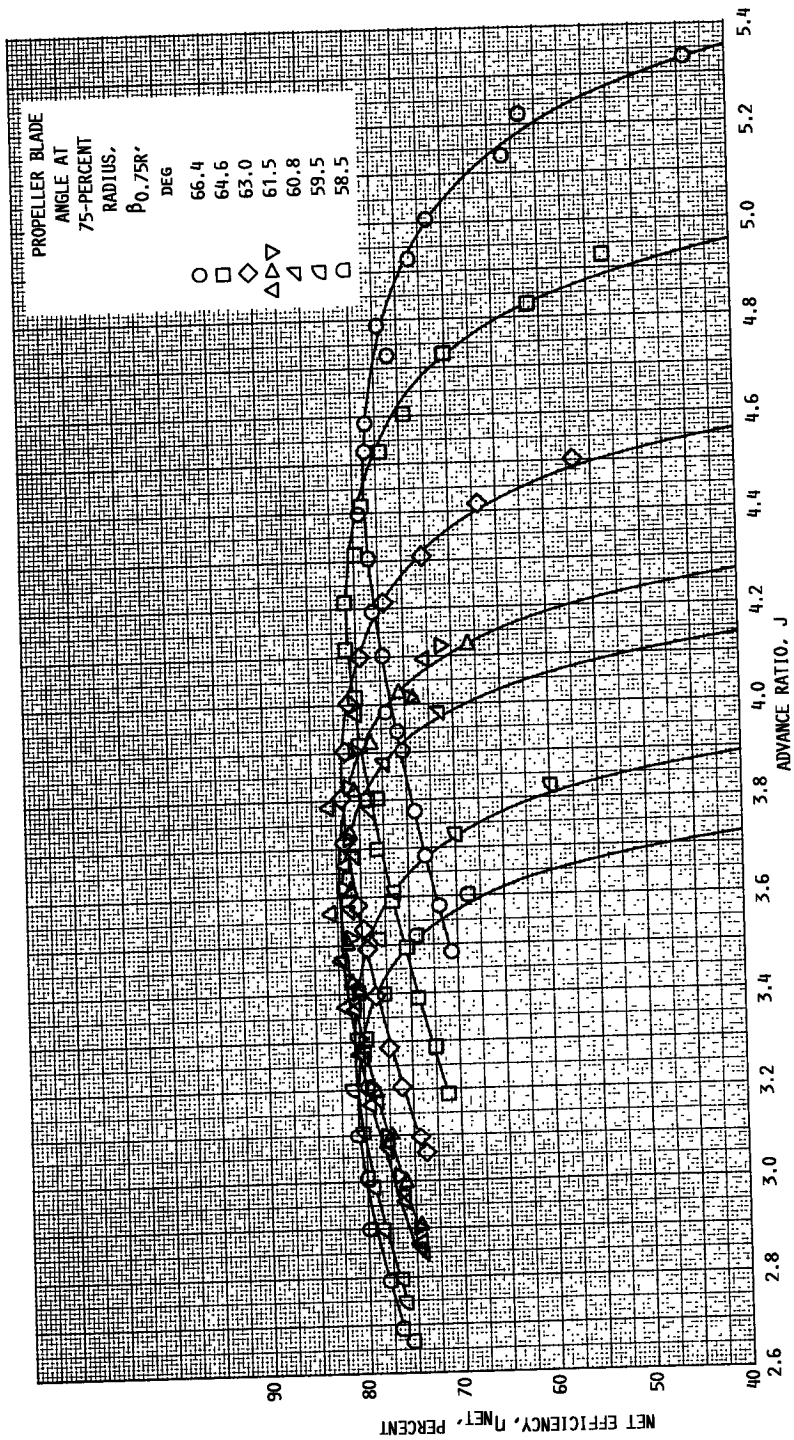

(b) NET EFFICIENCY; $M_0 = 0.6$.

FIGURE 10. - CONTINUED.

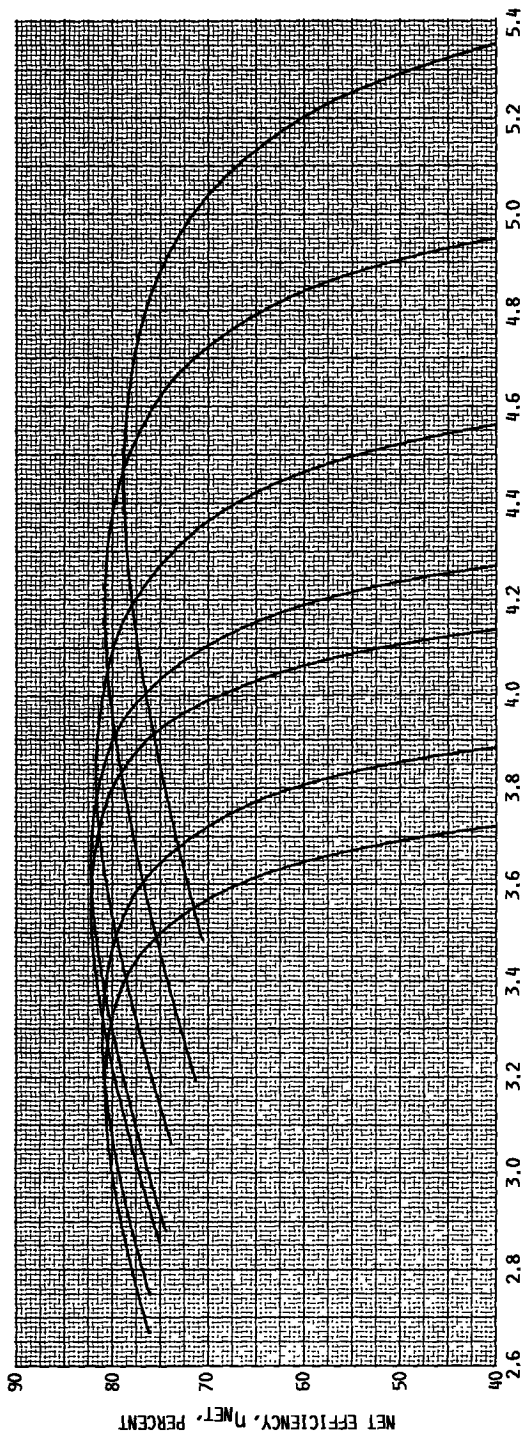

(c) NET EFFICIENCY FAIRING; $M_0 = 0.6$.

FIGURE 10. - CONCLUDED.

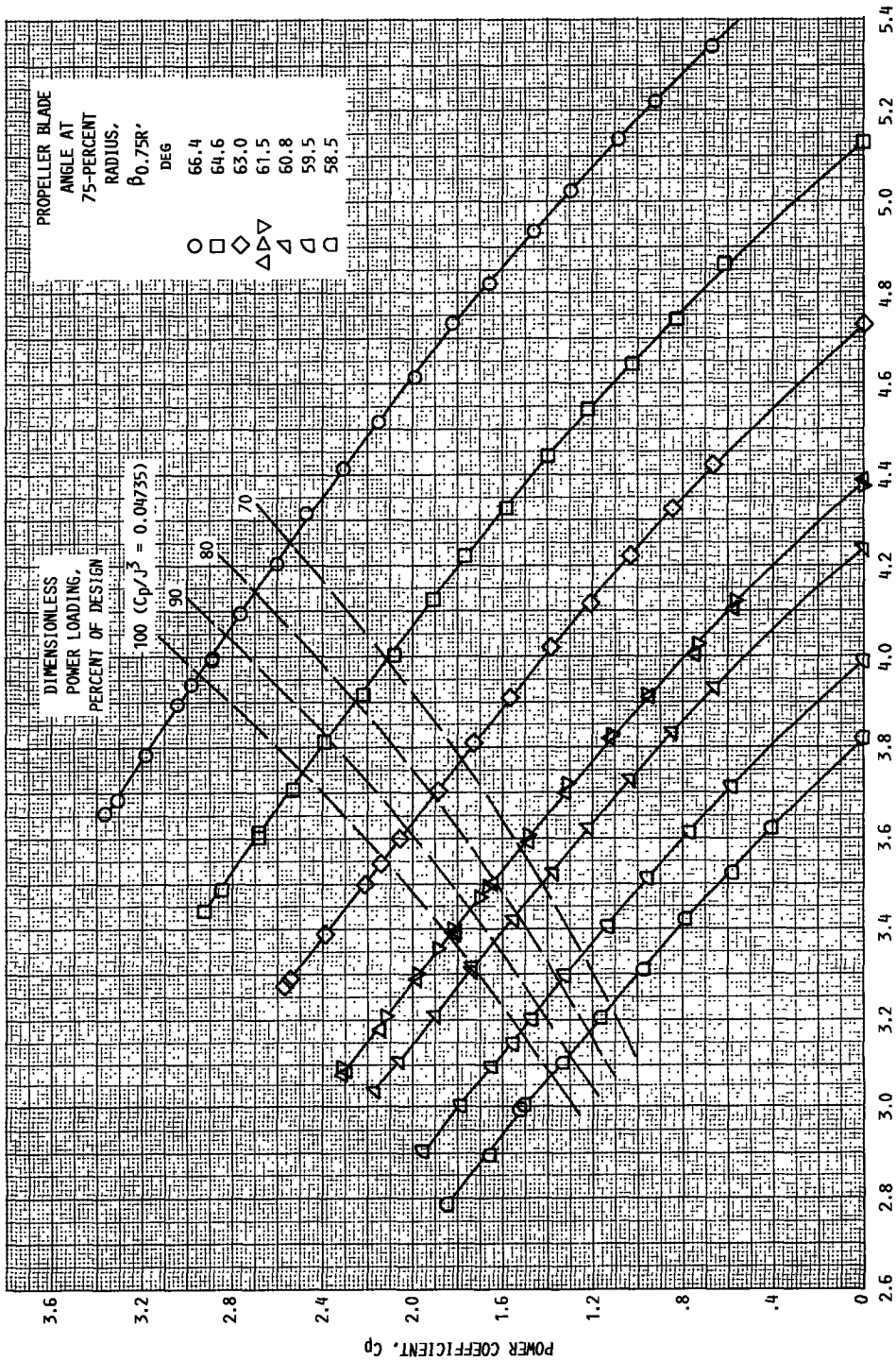

(a) POWER COEFFICIENT; $M_0 = 0.7$.

FIGURE 11. - MEASURED PROPELLER PERFORMANCE AT FREE-STREAM MACH NUMBER M_0 OF 0.7.

(b) NET EFFICIENCY; $M_0 = 0.7$.

FIGURE 11. - CONTINUED.

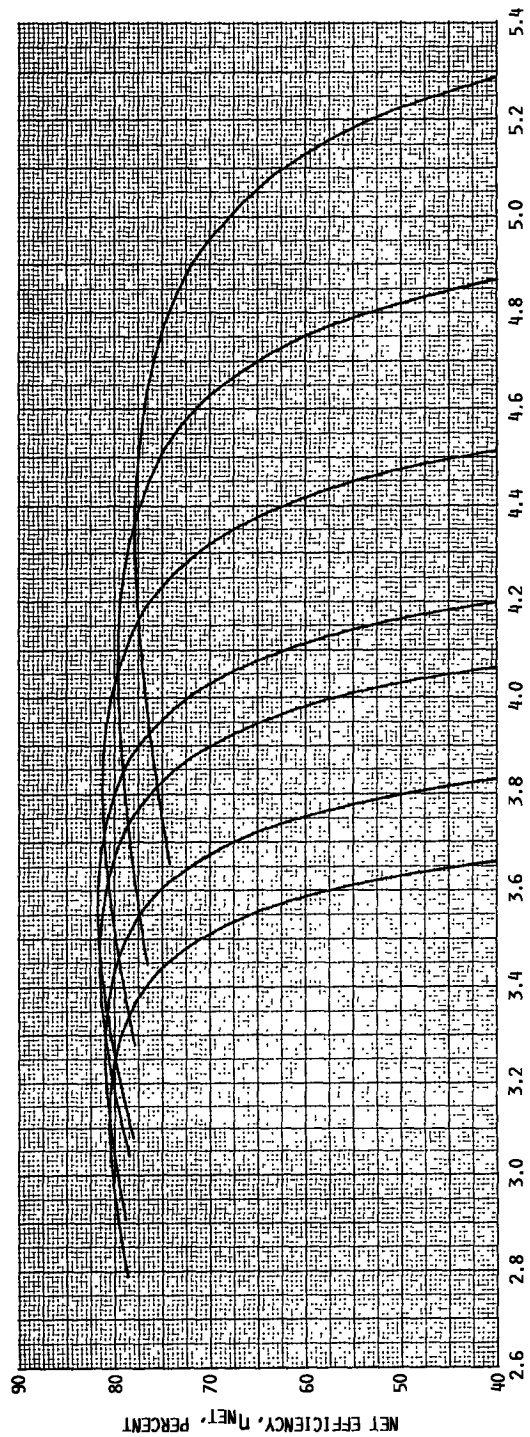

(c) NET EFFICIENCY FAIRING; $M_0 = 0.7$.

FIGURE 11. - CONCLUDED.

(a) POWER COEFFICIENT; M_0 = 0.75.

FIGURE 12. - MEASURED PROPELLER PERFORMANCE AT FREE-STREAM MACH NUMBER M_0 OF 0.75.

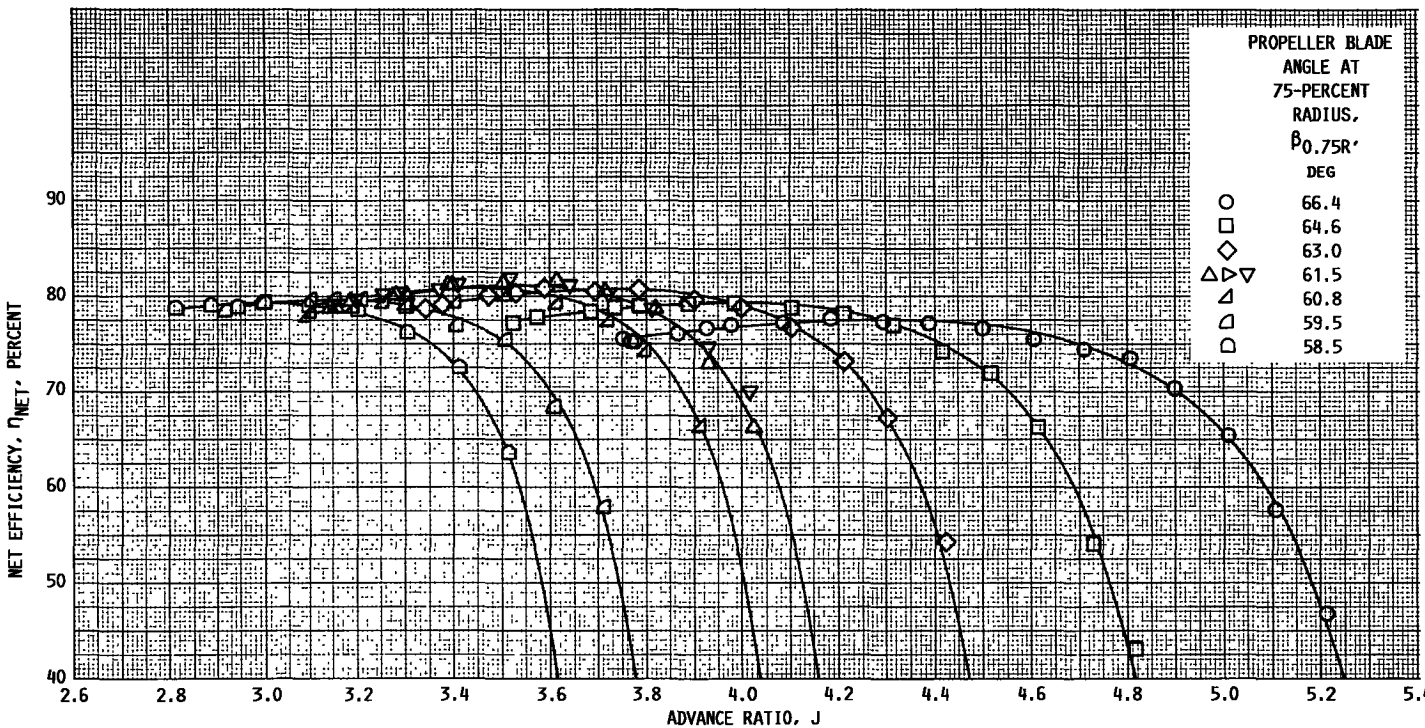

(b) NET EFFICIENCY; $M_0 = 0.75$.

FIGURE 12. - CONTINUED.

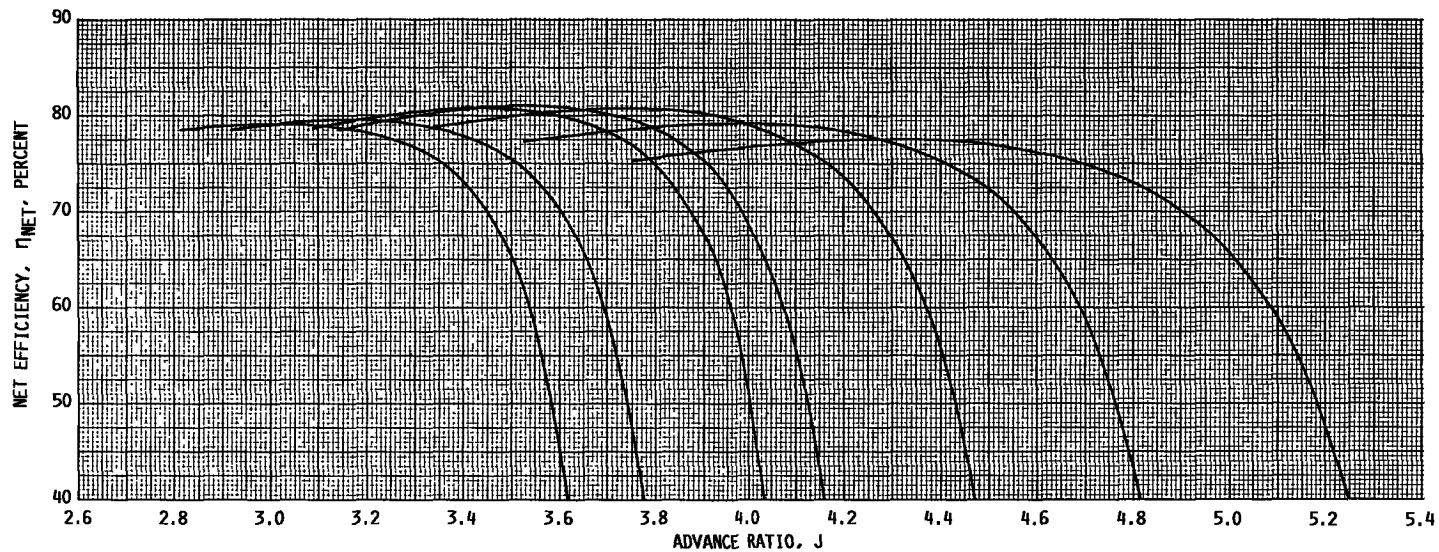

(c) NET EFFICIENCY FAIRING; M_0 = 0.75.

FIGURE 12. - CONCLUDED.

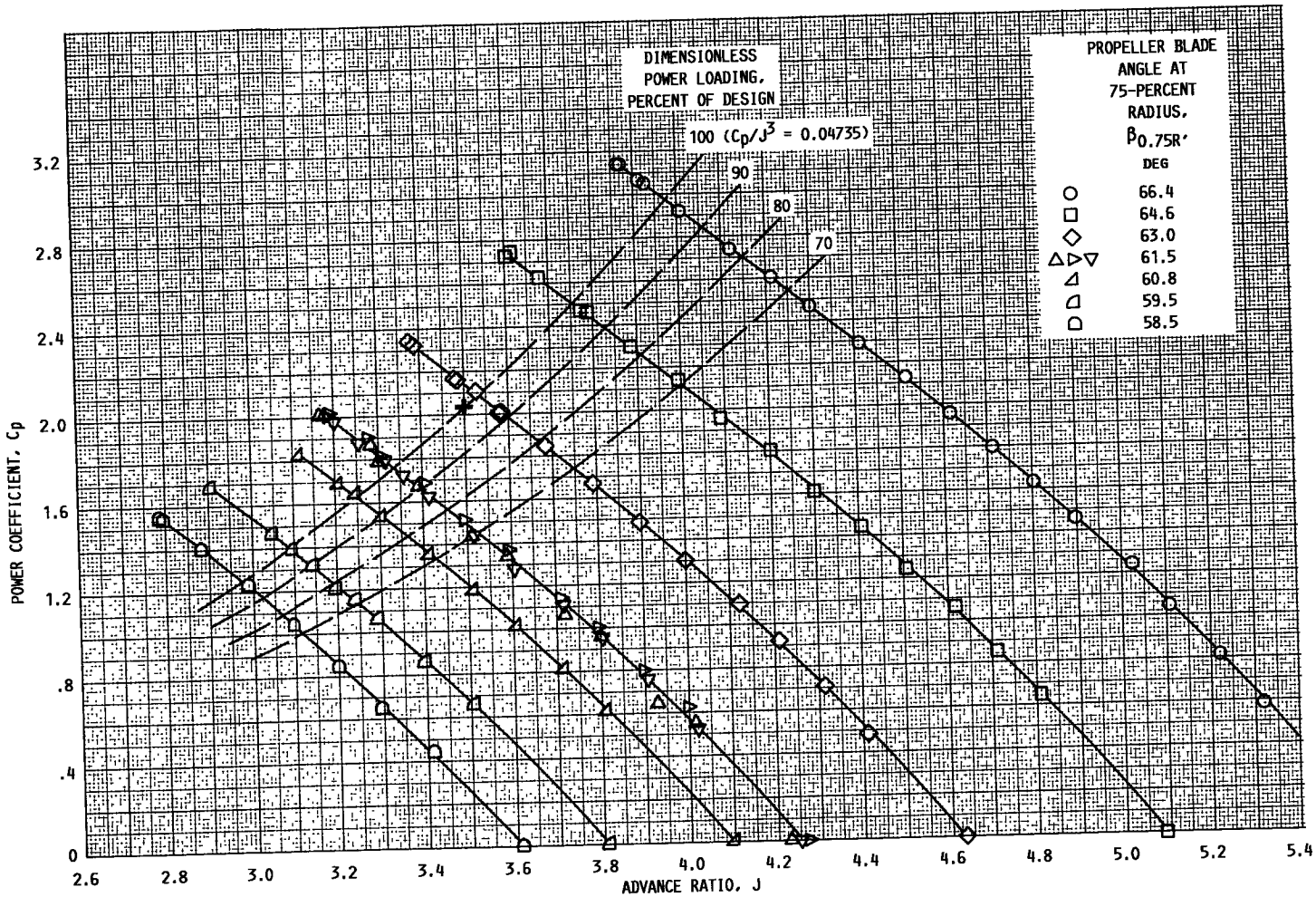

(a) POWER COEFFICIENT; M_0 = 0.8.

FIGURE 13. - MEASURED PROPELLER PERFORMANCE AT FREE-STREAM MACH NUMBER M_0 OF 0.8.

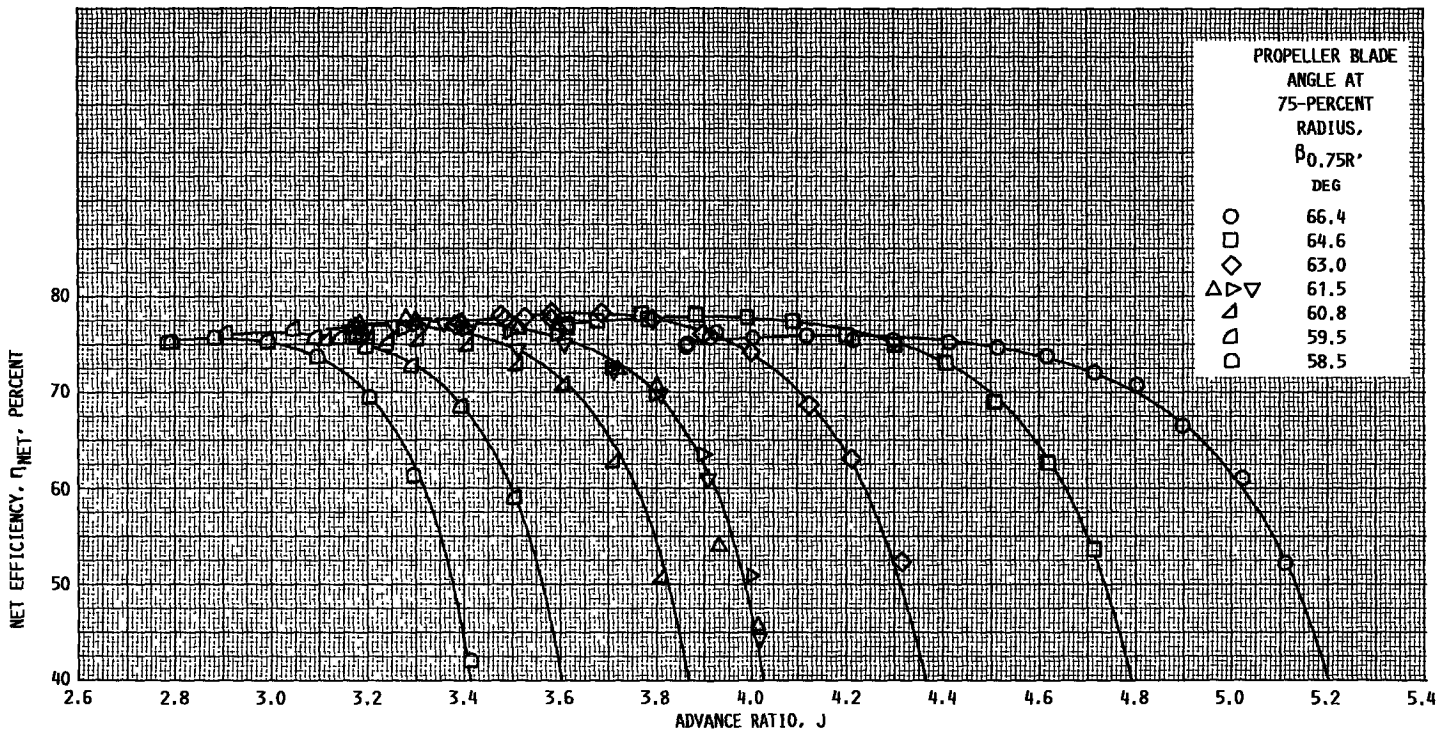

(b) NET EFFICIENCY; $M_0 = 0.8$.

FIGURE 13. - CONTINUED.

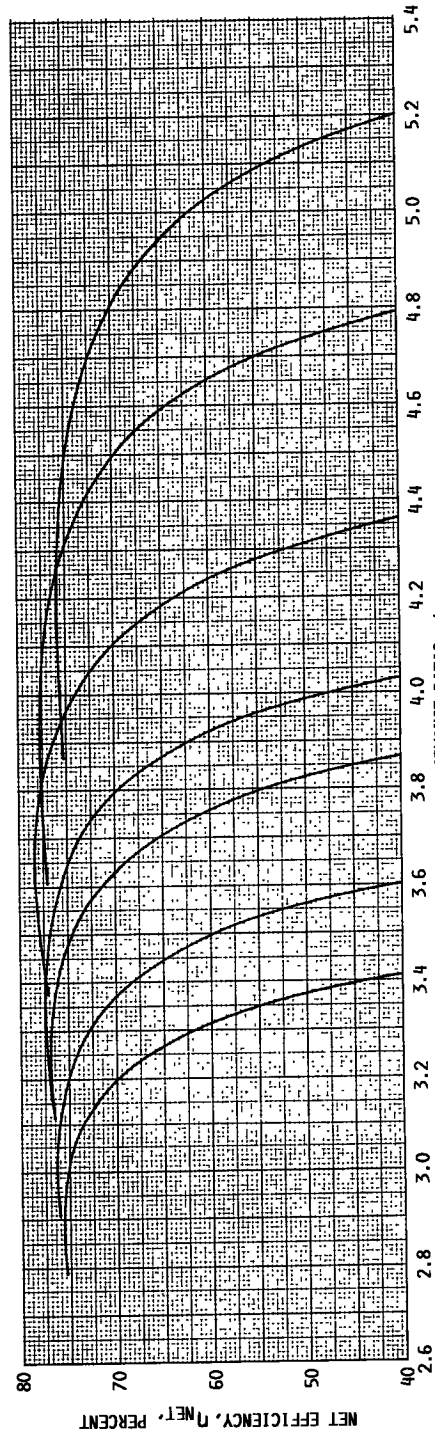

(c) NET EFFICIENCY FAIRING; $M_0 = 0.8$.

FIGURE 13. - CONCLUDED.

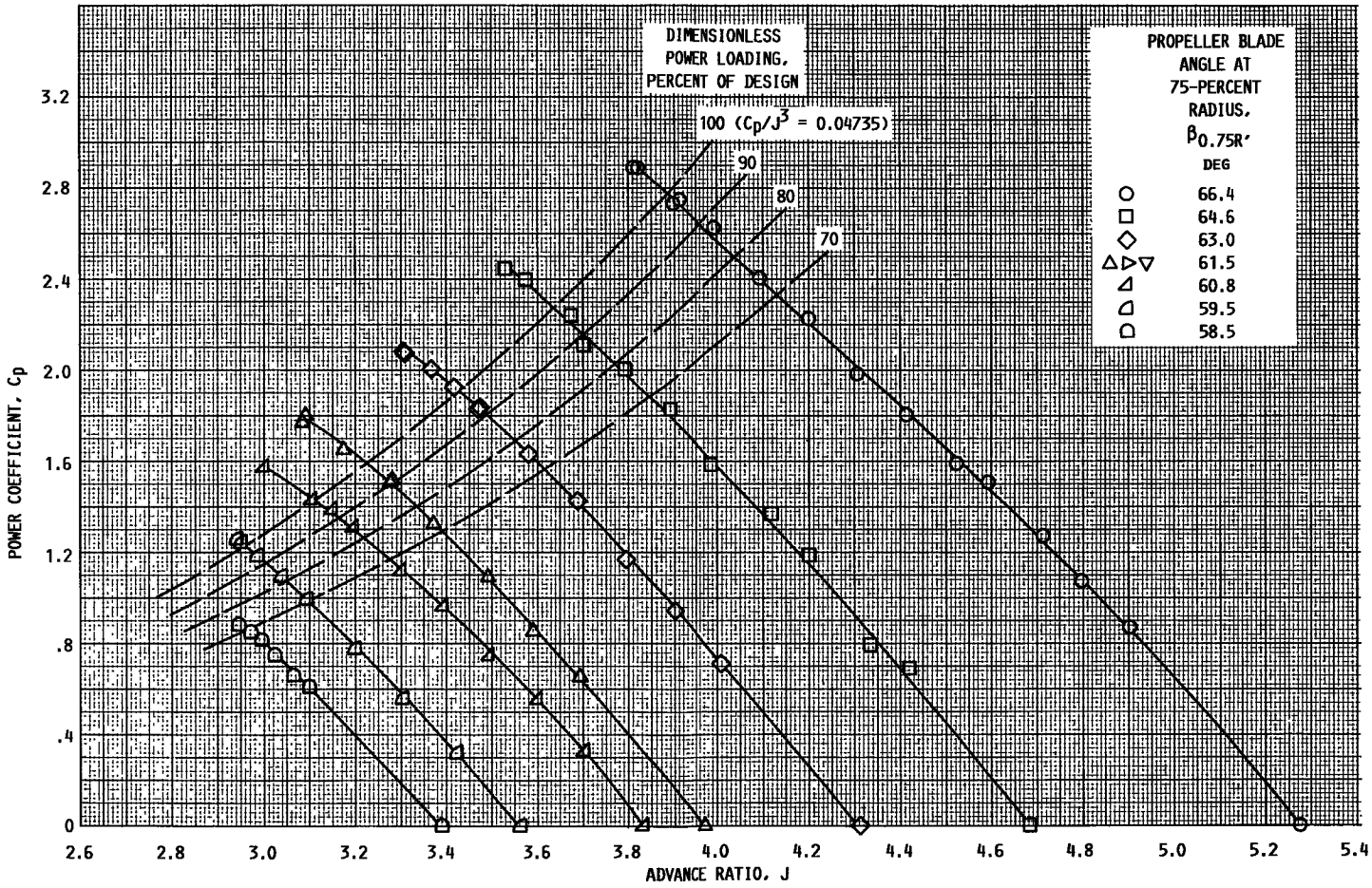

(a) POWER COEFFICIENT; M_0 = 0.85.

FIGURE 14. - MEASURED PROPELLER PERFORMANCE AT FREE-STREAM MACH NUMBER M_0 OF 0.85.

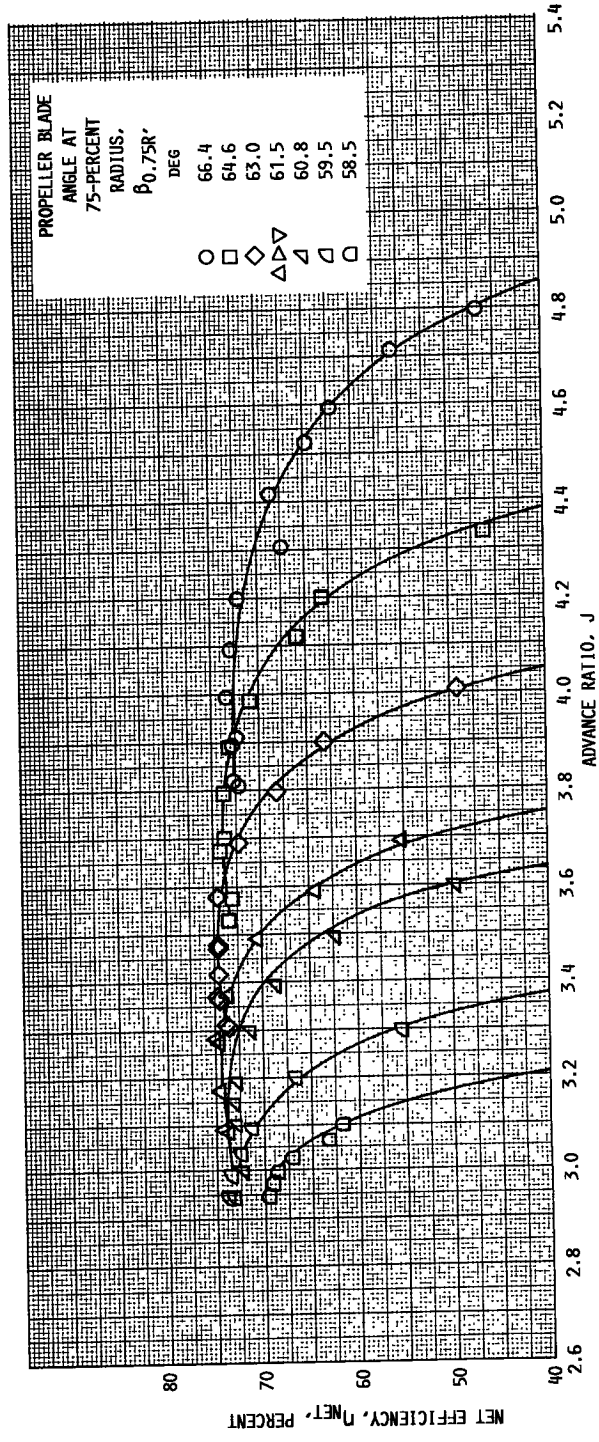

(b) NET EFFICIENCY; M_D = 0.85.

FIGURE 14. - CONTINUED.

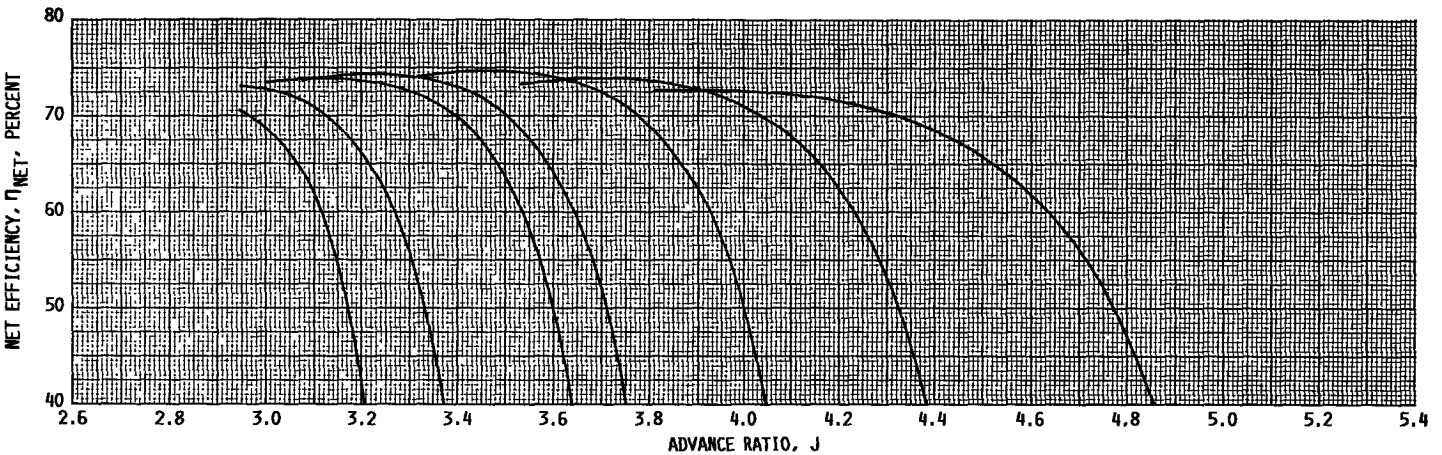

(c) NET EFFICIENCY FAIRING; $M_0 = 0.85$.

FIGURE 14. - CONCLUDED.

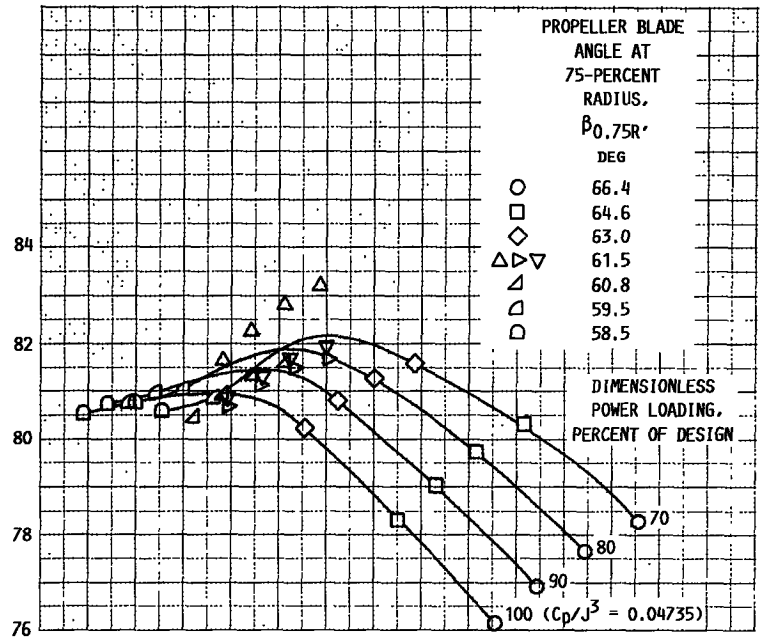

(a) FREE-STREAM MACH NUMBER M_0 OF 0.6.

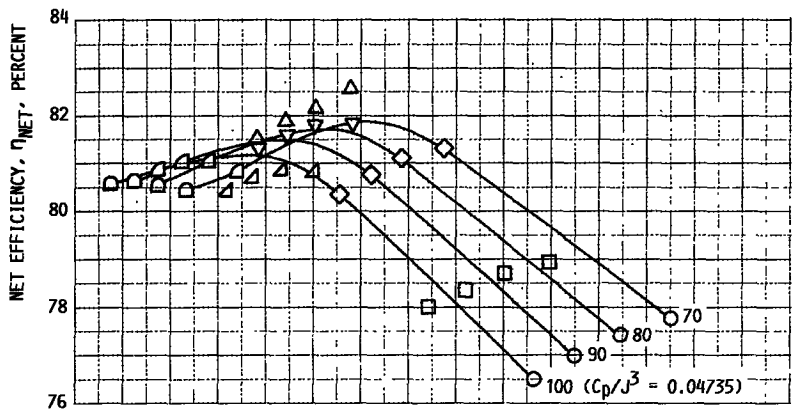

(b) FREE-STREAM MACH NUMBER M_0 OF 0.7.

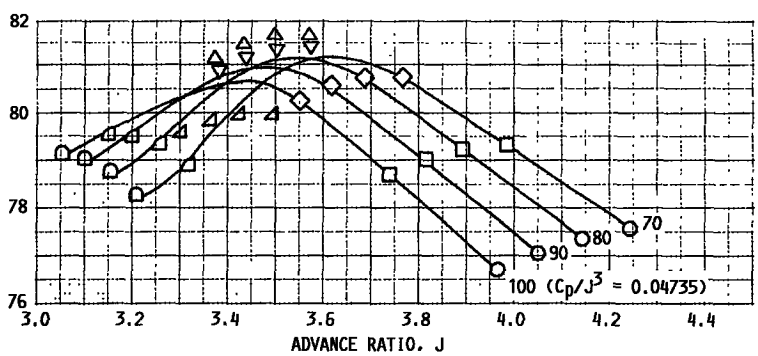

(c) FREE-STREAM MACH NUMBER M_0 OF 0.75.

FIGURE 15. - EFFECT OF POWER LOADING AND ADVANCE RATIO ON NET EFFICIENCY.

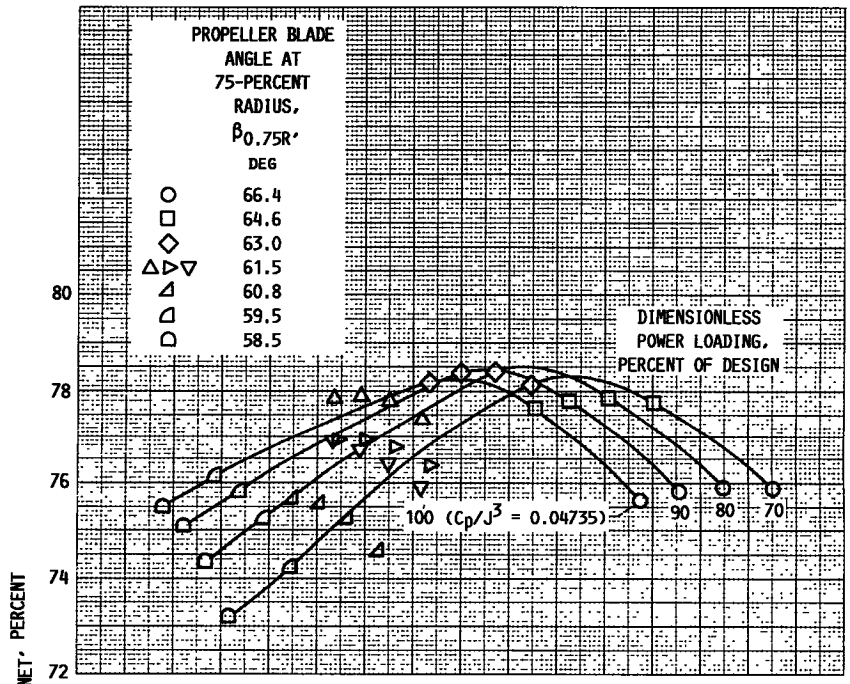

(d) FREE-STREAM MACH NUMBER M_0 OF 0.8.

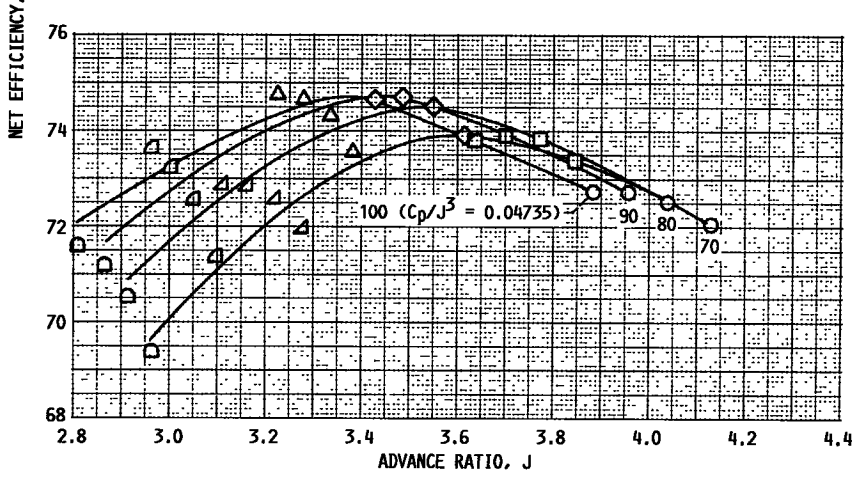

(e) FREE-STREAM MACH NUMBER M_0 OF 0.85.

FIGURE 15. - CONCLUDED.

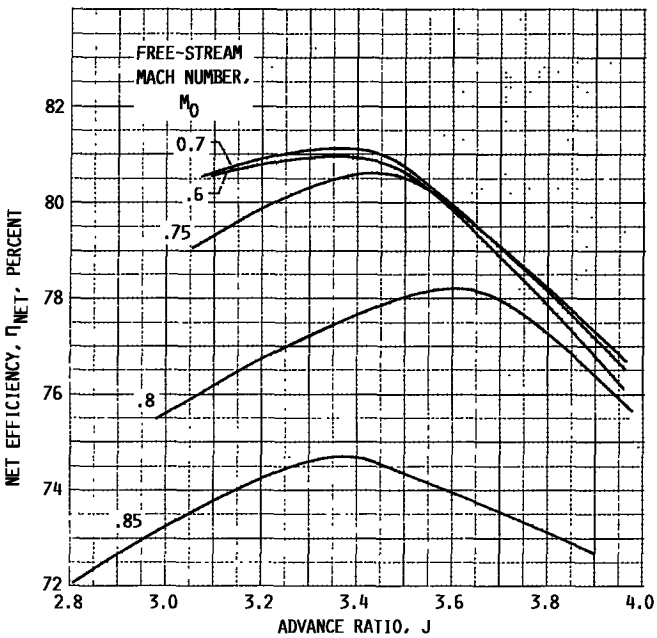

FIGURE 16. - EFFECT OF ADVANCE RATIO ON NET EFFICIENCY AT 100-PERCENT DIMENSIONLESS POWER LOADING.

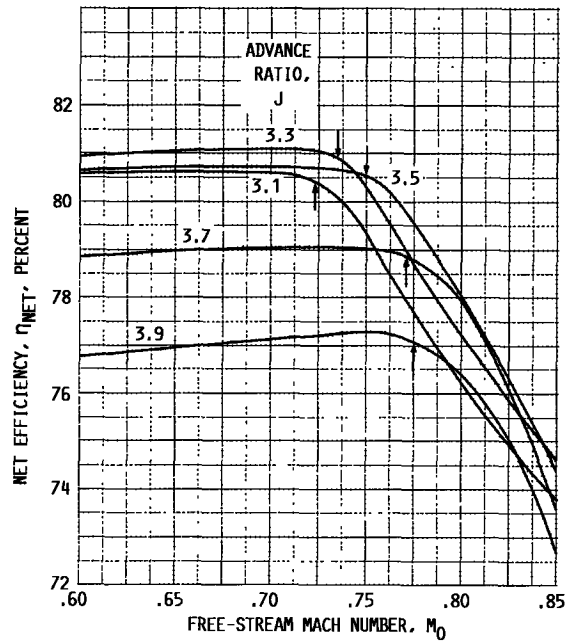

FIGURE 17. - EFFECT OF FREE-STREAM MACH NUMBER ON NET EFFICIENCY AT 100-PERCENT DIMENSIONLESS POWER LOADING.

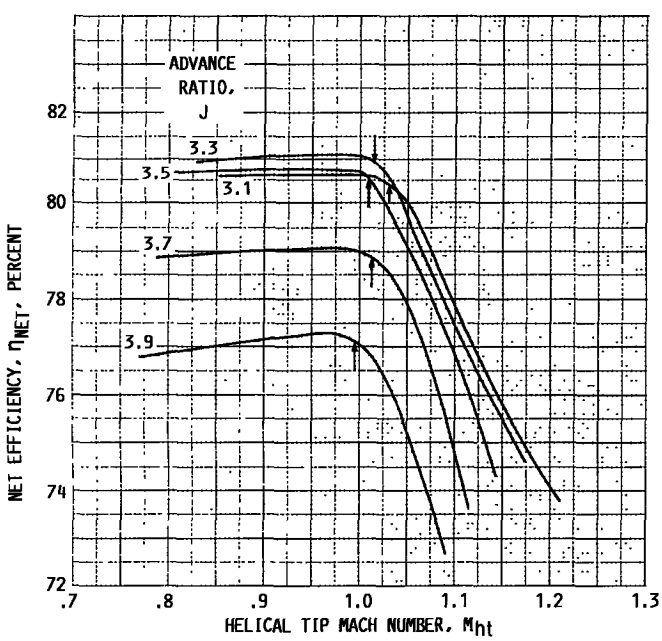

FIGURE 18. - EFFECT OF HELICAL TIP MACH NUMBER ON NET EFFICIENCY AT 100-PERCENT DIMENSIONLESS POWER LOADING.

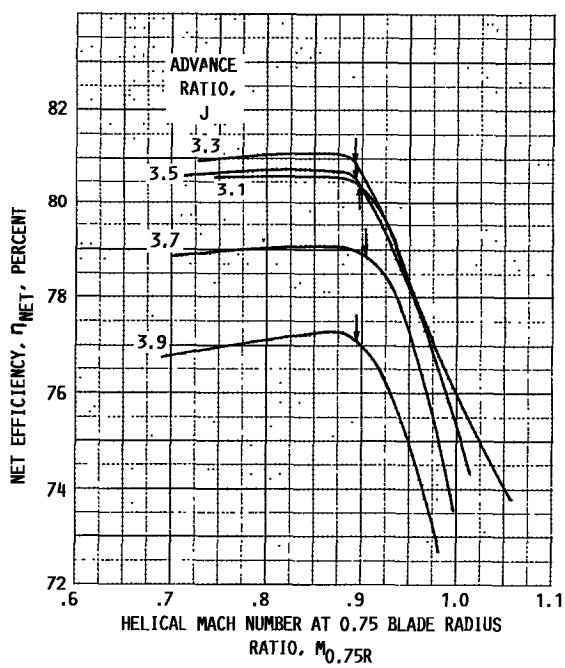

FIGURE 19. - EFFECT OF HELICAL MACH NUMBER AT 0.75 BLADE RADIUS RATIO ON NET EFFICIENCY AT 100-PERCENT DIMENSIONLESS POWER LOADING.

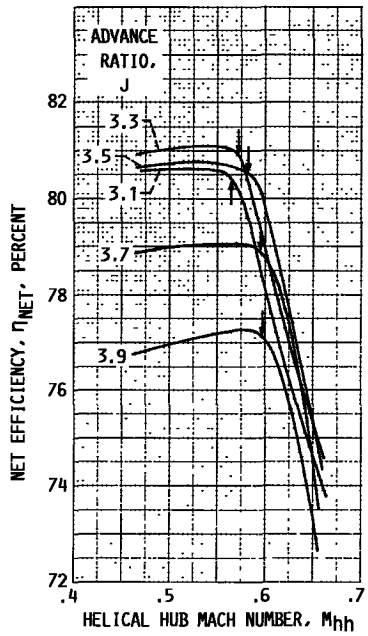

FIGURE 20. - EFFECT OF HELICAL HUB MACH NUMBER ON NET EFFICIENCY AT 100-PERCENT DIMENSIONLESS POWER LOADING.

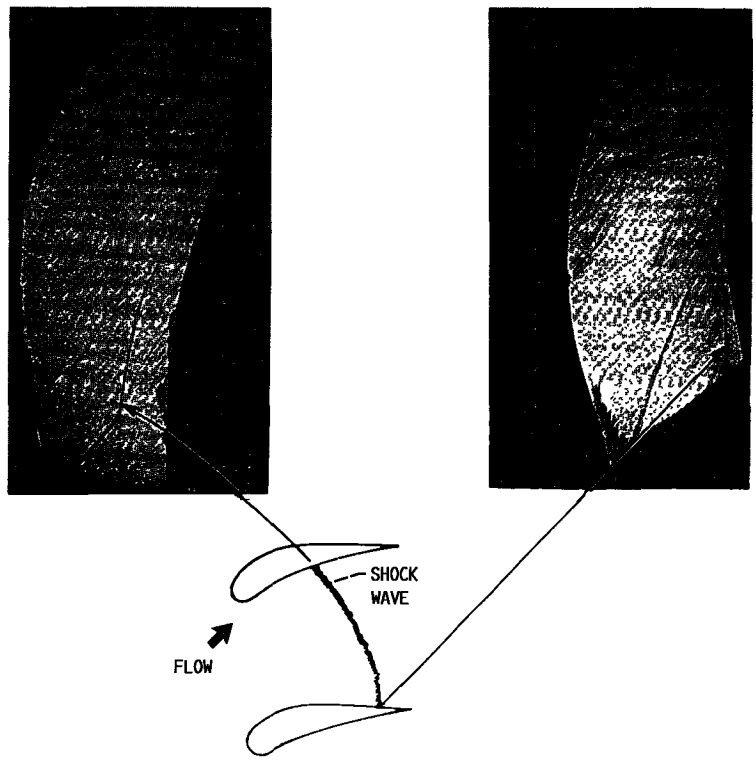

FIGURE 21. - RESULTS FROM PAINT FLOW VISUALIZATION TECHNIQUE INDICATING INTERBLADE SHOCK STRUCTURE AT FREE-STREAM MACH NUMBER OF 0.8.

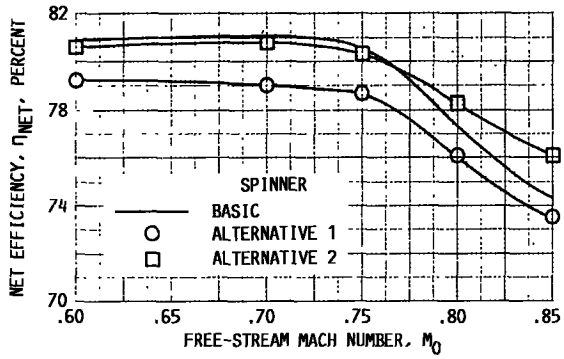

FIGURE 22. - NET EFFICIENCY MEASURED WITH ALTERNATIVE SPINNERS. DIMENSIONLESS POWER LOADING, 100 PERCENT; PROPELLER BLADE ANGLE AT 75-PERCENT RADIUS, $\beta_{0.75R}$, 61.5°.

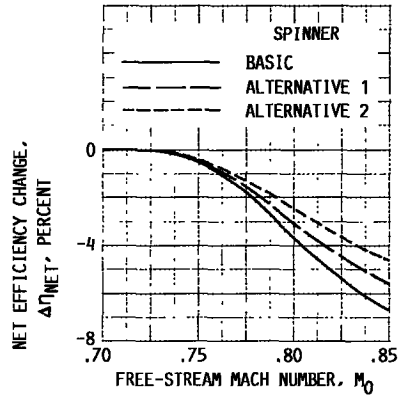

FIGURE 23. - ESTIMATED EFFECT OF ALTERNATIVE SPINNERS ON NET EFFICIENCY. DIMENSIONLESS POWER LOADING, 100 PERCENT; PROPELLER BLADE ANGLE AT 75-PERCENT RADIUS, $\beta_{0.75R}$, 61.5°.

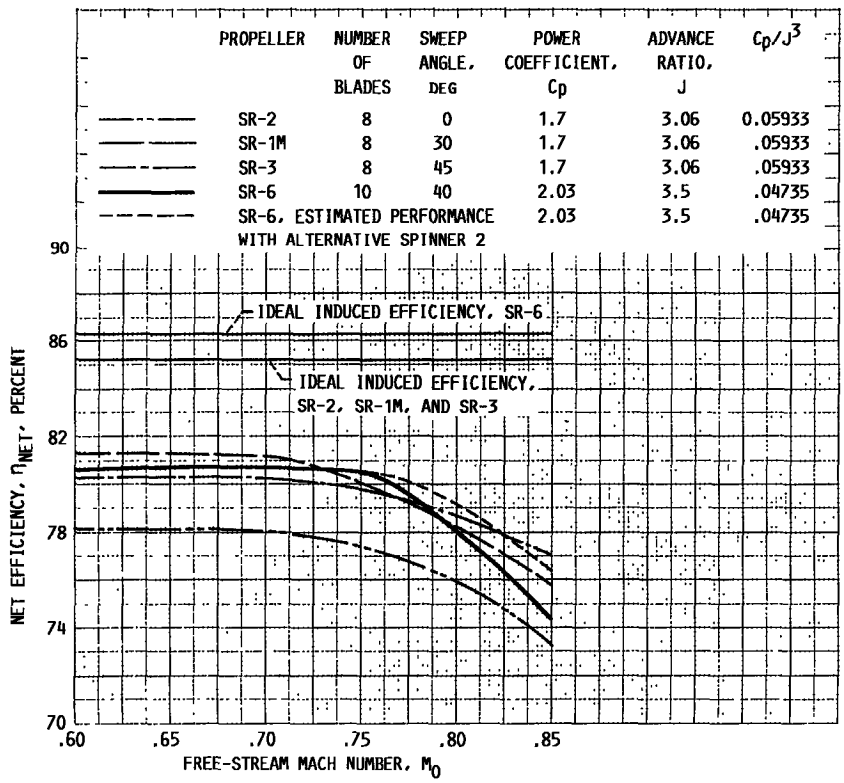

FIGURE 24. - COMPARISON OF PROPELLER PERFORMANCE.

NASA
National Aeronautics and Space Administration

Report Documentation Page

1. Report No.	2. Government Accession No.	3. Recipient's Catalog No.
NASA TM-88969		

4. Title and Subtitle

Experimental Aerodynamic Performance of Advanced 40°-Swept 10-Blade Propeller Model at Mach 0.6 to 0.85

5. Report Date

September 1988

6. Performing Organization Code

7. Author(s)

Glenn A. Mitchell

8. Performing Organization Report No.

E-3437

10. Work Unit No.

535-03-01

9. Performing Organization Name and Address

National Aeronautics and Space Administration
Lewis Research Center
Cleveland, Ohio 44135-3191

11. Contract or Grant No.

13. Type of Report and Period Covered

Technical Memorandum

12. Sponsoring Agency Name and Address

National Aeronautics and Space Administration
Washington, D.C. 20546-0001

14. Sponsoring Agency Code

15. Supplementary Notes

16. Abstract

A propeller designated as SR-6, designed with 40° of sweep and 10 blades to cruise at Mach 0.8 at an altitude of 10.7 km (35 000 ft), was tested in the NASA Lewis Research Center's 8- by 6-Foot Wind Tunnel. This propeller was one of a series of advanced single-rotation propeller models that were designed and tested as a part of the NASA Advanced Turboprop Project. Design-point net efficiency was almost constant to Mach 0.75 but fell above this speed more rapidly than that of any previously tested advanced propeller. Alternative spinners that further reduced the near-hub interblade Mach numbers and relieved the observed hub choking improved performance above Mach 0.75. One spinner attained estimated SR-6 design-point net efficiencies of 80.6 percent at Mach 0.75 and 79.2 percent at Mach 0.8, higher than the measured performance of any previously tested advanced single-rotation propeller at these speeds.

17. Key Words (Suggested by Author(s))	18. Distribution Statement
Advanced turboprop; Propeller; Energy efficient; Propfan	Unclassified - unlimited Subject Category 02

19. Security Classif. (of this report)	20. Security Classif. (of this page)	21. No of pages	22. Price*
Unclassified	Unclassified	42	A03

NASA FORM 1626 OCT 86

*For sale by the National Technical Information Service, Springfield, Virginia 22161